CALIBRATION-FREE GAZE TRACKING

By

William Maio

A Thesis Submitted to the Graduate

Faculty of Rensselaer Polytechnic Institute

in Partial Fulfillment of the

Requirements for the Degree of

MASTER OF SCIENCE

Major Subject: ELECTRICAL ENGINEERING

Approved:

_____

Qiang Ji, Thesis Adviser

Rensselaer Polytechnic Institute
Troy, New York

December 2011

CONTENTS

LIST OF TABLES

LIST OF FIGURES

ACKNOWLEDGMENT

I wish to express my sincere appreciation to my research advisor, Professor Qiang Ji, for his guidance, inspiration, wisdom, patience, humor, and above all, his encouragement through my graduate studies. He has been a passionate mentor who helped me further develop my research skills and overcome my shortcomings. I thank his consistent faith in me throughout the research, especially during the toughest times. I would also like to thank the current and previous members of the RPI Intelligent Systems Lab for their friendship inside and outside of the lab, especially, my senior lab mate, Dr. Jixu Chen, for his insightful comments and suggestions during our research discussions.

I would also like to thank all my friends that I met throughout my life. Your kindness and help have shaped the person I am today. I dedicate this thesis to my family, especially my parents, Sherby Miao, and Marina Wu for their unconditional love and support during the good times and bad times in my life. Without them, none of my accomplishments would have been possible.

ABSTRACT

The application of gaze tracking is well established in user behavior studies and human computer interface for some applications such as amyotrophic lateral sclerosis patients. However, those application of gaze tracking is still limited in other domains due to various challenges. One of the challenges is the cumbersome calibration process that requires the user to gaze at calibration points on an object, typically a monitor screen. This process is necessary to estimate the subject specific eye parameters, which are essential to model the eye in 3D and to estimate the gaze accurately. In this thesis, we focus on improving the calibration process by eliminating the need for explicit calibration. This improvement simplifies the use by reducing the user's effort for calibration. This is particularly important for three reasons. First, the calibration process tends to discourage the user from using the technology and influences the user's state of mind in a user behavior study. Second, it prevents the development of a fully automatic and natural eye tracking system. Third, the system cannot estimate the user's gaze accurately when the user is uncooperative, which is particularly true if the user is an infant or a criminal. In this thesis, we take two approaches to solve this problem.

First, we extend and improve an existing stereo eye tracking approach that does not require explicit personal calibration. This approach eliminates the need for explicit calibration by exploiting the binocular constraint that assumes visual axes of the two eye intersects at the gaze point. However, this approach, being very susceptible to image noise, is neither robust nor accurate enough for practical applications. To alleviate this problem, we propose to enhance this method with two additional constraints: the screen constraint and the eye parameter constraint. While the former limits the scope of the eye gaze, the latter limits the range of the eye parameters. Experiments show that the proposed enhancements improve both the gaze estimation accuracy and robustness, as well as simplify its use.

Second, we study the feasibility of performing calibration-free eye gaze tracking from a monocular camera. Compared to the stereo eye gaze tracking, the monoc-

ular eye tracking allows larger head movement. In order to realize this approach, we systematically develop a mathematical model that for the first time establishes a concise analytic relationship between the optical axis, the visual axis and the personal eye parameters. Using this mathematical model, we show that a measurement matrix resulting from a collection of optical axes can be constructed, and furthermore we show that the measurement matrix can be factorized into the product of two matrices- one is composed of the visual axes and another composed of the personal parameters only. Based on this, we propose a factorization procedure that can recover the personal parameters (up to a rotation matrix) by factorizing the measurement matrix through singular value decomposition. Further research is needed to estimate the rotational matrix and to validate the method.

CHAPTER 1
Introduction

1.1 Overview

From recent research and development in human computer interface (HCI), Microsoft Kinect [15] completely redefines the conventional HCI (keyboard and mouse) available to the mass-consumer market. This new type of advanced human computer interface, so-called "natural user interface" (NUI), enables the users to naturally interact with the computer system through gestures. This type of interface merely existed in science fiction as featured in the science fiction film *Minority Report* [16], but research and development has made it a reality.

Similarly, eye/gaze tracking is another advanced HCI that is being developed. Via this advanced HCI, eye/gaze tracking in the science fiction film, *Iron Man* [5], is applied as a targeting system for Iron Man's head up display (HUD). Although the technology is not as well-developed as portrayed in the film, gaze tracking has been well-established in certain niche applications such as eye-controlled mouse pointer for amyotrophic lateral sclerosis patients and user behavior studies. Several commercial companies such as Tobii [21] have developed products for those applications. However, both of those applications require a specialized system that costs in the order of thousands US dollars and a cumbersome calibration for each user. Recent development has brought the cost of the technology of the device down for developers. The open-source hardware and software gaze tracking project, EyeWriter Initiative, costs only 100 dollars [20]. However, the cumbersome calibration process is still a problem that is preventing gaze-tracking from being widely used like keyboard and mouse for three reasons. First, the calibration process tends to discourage the user from using the technology and influences the user's state of mind in a user behavior study. Second, it prevents the development of a fully automatic and natural eye tracking system. Third, the system cannot estimate the user's gaze accurately when the user is uncooperative, which is particularly true if the user is an infant or a criminal. In this thesis, we take two approaches to solve this problem.

1.2 Historical Review and Problem Statement

Traditional eye gaze tracking methods can be divided into the 2D methods and the 3D methods. The 2D approach learns a polynomial mapping function from the 2D features (e.g. 2D pupil glint vector) [8], [12], [13] , [22] or 2D eye images [19] to gaze point on the screen. However, the 2D mapping approach has two common drawbacks: First, in order to learn the mapping function, the user has to perform complex experiment to calibrate the parameters of the mapping functions. For example, in the calibration procedure of [9], the subject needs to gaze at 9 evenly distributed points on the screen or gaze at 12 points for higher accuracy. Second, because the extracted 2-D eye image features vary significantly with head position, the gaze mapping function is very sensitive to head motion. In [13], they report detailed data showing how the gaze tracking system decay as the head moves away from original calibration position. Hence, the user has to keep his head unnaturally still in order to achieve good performance. Methods have also been proposed to handle head pose changes using Neural Network [8] or SVM [22]. These methods, however, either only consider the in-plane head translation [8] or need complex stereo cameras to obtain the 3D eye position [22].

Different from the 2D mapping-based gaze estimation, the 3D gaze estimation is based on high resolution stereo cameras [1], [4], [6], [14] or single camera with multiple calibrated light sources [7] to estimate 3D eye features (the corneal curvature center, the pupil center, and the optical axis connecting them) directly by the 3D reconstruction technique. Then, the visual axis is estimated from the 3D features, and the gaze point on the screen is obtained by intersecting the visual axis with the screen. However, this kind of method still needs the person-specific calibration to estimate the eye parameters. For example, Guestrin et al. [6] propose to estimate 3D gaze with the use of stereo camera and multiple IR lights. Their method starts with the reconstruction of the optical axis of the eye. The visual axis can be estimated by adding a constant angle to the optical axis. However, the angle between visual axis and optical axis needs to be estimated beforehand through a personal calibration procedure. Most recently, gaze estimation methods are proposed without active calibration. Sugano et al. [18], [17] proposed "implicit"

calibration methods for 2D based gaze estimation. These methods still need to collect the gaze points as training data. However, it collects the gaze point implicitly, i.e. the user is unconscious of this process while working normally and naturally with the eye tracking system. In [18], they collect gaze points implicitly by assuming the subject is looking at the cursor on the screen when he/she clicks the mouse. However, it still needs active user participation. In [17], gaze points are collected when the subject is watching an image or video in the monitor. Given the saliency map of the image, gaze points are sampled from it and used as training data to train a mapping function (Gaussian Process Regresser) between eye image and gaze point. However, the method is not robust, very susceptible to image noise. because of the large uncertainty in saliency map, the accuracy of this system is pretty low (6 degrees) comparing with state-of-the-art (<1 degree). Furthermore, since this is basically a 2D mapping method which doesn't consider head pose, a chin rest is used to fix the head. Jixu et al. [3] has proposed an incremental implicit calibration process with probabilistic representation of the gaze utilizing saliency map for the 3D eye model. However, the saliency map of the scene is needed for this approach.

Without collecting any gaze points, Model and Eizenman [11] propose to estimate the eye parameters directly from anatomical knowledge. However, because of the noise in optical axis, it's difficult to achieve accurate result. For standard 40 cm by 30 cm flat monitor, when the noise in the optical axis is 0.4 degrees, the estimation error is 2.6 degree; when the optical noise is 1 degree, the error over 5 degrees. Although they propose to use a larger monitor (160 cm by 120 cm) or pyramid observation surface to reduce the error, they are usually not available in real applications.

In this thesis, we introduce two different approaches to eliminate the need for explicit calibration. First, alleviating the problem with Model's binocular constraints approach [11], we introduce two additional constraints [10] to enhance this method. Second, taking a new calibration-free approach, we developed a framework that utilizes the factorization of eye measurement matrix to recover the subject specific parameters.

1.3 Structure of the Thesis

The thesis is structured as follows. Chapter 2 presents the 3D eye model and the explicit personal parameter calibration process. Chapter 3 presents the implicit constraint-based calibration process. Chapter 4 presents the calibration-free approach with the factorization of the eye measurement matrix. Conclusions will be drawn in chapter 5.

CHAPTER 2
3D Eye Model Gaze Estimation

2.1 3D Eye Model

In the 3D eye model, one's gaze is modeled as a line in 3D called visual axis that intersects with fovea (f), and corneal curvature center (c). The intersection between the visual axis and the object being looked at is the gaze point. The following figure illustrates the traditional eye model [7].

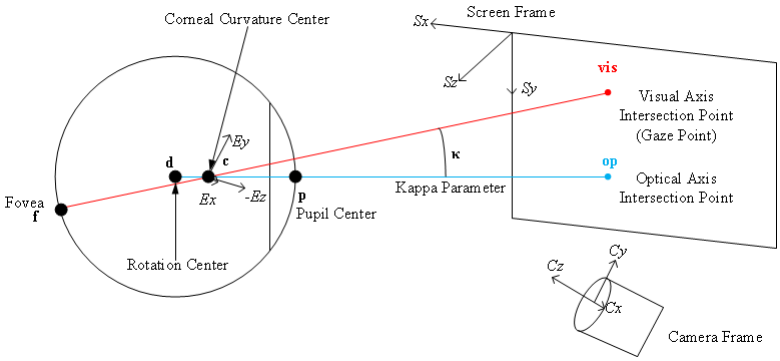

Figure 2.1: Eye Model

In figure 2.1, the red line that intersects the fovea (f) and the corneal curvature center (c), is the visual axis ($\vec{vis}$). Three different frames are defined to reference the position and orientation of different components in the gaze tracking system. The origin of the camerae frame (C_x, C_y, C_z) is the optical center of the camera, and the direction of C_z is the optical axis of the camera. The origin of the screen frame (S_x, S_y, S_z) is the top left corner of the screen, and the direction of S_z is the normal of the screen plane. The origin of the eye model frame is the corneal curvature center, and the direction of E_z is opposite of C_z while the other two axes have the same orientation. The intersection of the visual axis with the screen frame is the gaze point (vis). The goal of gaze tracking is to estimate vis. The gaze point is also used as a calibration point. The camera frame is used to reference the 3D position of the components in the eye model. The screen frame is used to reference the intersection points to the relative 2D coordinates on the monitor

screen. The relative pose between the camera frame and the screen frame, a rotation and a translation, is estimated through a system calibration using computer a vision technique with a mirror.

The following table summarizes each of the components in the gaze tracking model.

Table 2.1: List of Eye Parameters in the 3D Eye Model

Symbol	Name	Note
c	Corneal Curvature Center	3D point that intersects with $\vec{vis}$ and $\vec{op}$
p	Pupil Center	3D point that intersects with $\vec{op}$
f	Fovea	3D point that intersects with $\vec{vis}$
$\vec{op}$	Optical Axis	Orientation of op with θ and ϕ
$\vec{vis}$	Visual Axis	Orientation of vis with $\theta + \alpha$ and $\phi + \beta$
op	Optical Axis intersection	Intersection point of $\vec{op}$ with K line parameter
vis	Visual Axis intersection	Intersection point of $\vec{vis}$ with λ line parameter

The optical axis of the eye is the line that pass through the corneal curvature center (c), and the pupil center (p).[1] In the 3D eye model, instead of modeling the position of fovea, the visual axis is directly modeled from the optical axis ($\vec{op}$) with an angle deviation (κ). The position of those two points can be estimated via a combination of biological properties of the eye, active lights and computer vision techniques. Note that the position of c, f, p moves when the orientation or the position of the eye changes. The relationship between the optical axis and visual axis modeled in the eye model frame (E_x, E_y, $-E_z$) is illustrated in the figure below.

[1] In the rest of this thesis, the optical axis refers to the optical axis of the 3D eye model, and not the optical axis of the camera.

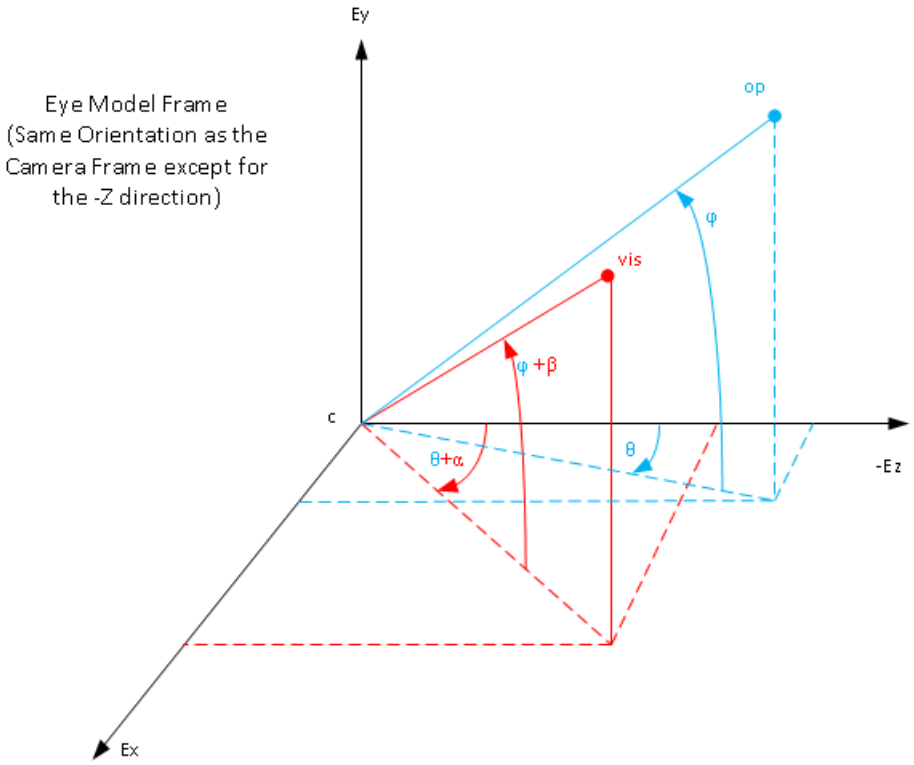

Figure 2.2: Angle Representation of Optical axis, $\vec{op}$, and Visual Axis, $\vec{vis}$

.

As noted in figure 2.2, the eye model frame has the same orientation as the camera frame except the $-z$ axis. The orientation of the optical axis is modeled with pan (horizontal) angle ϕ and tilt (vertical) angle θ in the eye model frame. Based on figure 2.2 The following equation describes the orientation of the optical axis.

$$\vec{op} = \begin{pmatrix} \cos(\phi)\sin(\theta) \\ \sin(\phi) \\ -\cos(\phi)\cos(\theta) \end{pmatrix} \tag{2.1}$$

The orientation of the visual axis is modeled with subject specific parameter κ that is a function of pan angle α and tilt angle β, which are added to the optical axis angles (θ and ϕ). The following equation describes the orientation of the visual axis.

$$\vec{vis} = \begin{pmatrix} \cos(\phi+\beta)\sin(\theta+\alpha) \\ \sin(\phi+\beta) \\ -\cos(\phi+\beta)\cos(\theta+\alpha) \end{pmatrix} \tag{2.2}$$

From the two axes, $\vec{op}$ and $\vec{vis}$, we can find the intersection point with the screen frame represented by op and vis. op, the optical axis intersection point is given in the following equation,

$$op = c + K \begin{pmatrix} \cos(\phi)\sin(\theta) \\ \sin(\phi) \\ -\cos(\phi)\cos(\theta) \end{pmatrix} \tag{2.3}$$

where c is the corneal curvature center. K is the line parameter that determines the position of the intersection point. ϕ and θ are the angles that describe the orientation of the optical axis from equation (2.1). Similarly, vis, the visual axis intersection point (true gaze point), is given in the following equation,

$$vis = c + \lambda \begin{pmatrix} \cos(\phi+\beta)\sin(\theta+\alpha) \\ \sin(\phi+\beta) \\ -\cos(\phi+\beta)\cos(\theta+\alpha) \end{pmatrix} \tag{2.4}$$

where c is the corneal curvature center. λ is the line parameter that determines the position of gaze. $\phi+\beta$ and $\theta+\alpha$ are the angles that describe the orientation of the visual axis from equation (2.2).[2]

2.2 Explicit Personal Calibration Process

The conventional method to estimate the subject specific parameters α and β from equation (2.2) and (2.4) is the 9-point calibration process. This process requires the user to sequentially gaze at 9 different points on the screen. Then, optimization techniques are applied to estimate α and β that minimize the deviation between the

[2]Note that the subject specific parameter (α and β) remains constant for each individual user, invariant of the gaze orientation.

actual gaze and the estimated gaze. The objective function of the optimization is the following equation.

$$f_{obj}(\alpha, \beta) = \sum_{i=1}^{i=9} \|G_i(\theta_i, \phi_i, \alpha, \beta) - C_i\|_2^2 \tag{2.5}$$

Both, G_i and C_i are points on the screen relative to the left top corner in the screen frame from figure 2.1. G_i is the estimated visual axis intersection point and C_i is the calibration point. The point index, i , is the reference to each of the 9 calibration points.

CHAPTER 3
Constraint-based Implicit Calibration Process

3.1 Introduction

In this chapter, the enhancement to the existing stereo eye tracking approach with constraints is presented. First, the existing framework with the binocular constraint proposed by Model et al.[11] is presented in section 3.2.1. In section 3.2.2 and 3.2.3, the proposed constraints [10] that enhance the approach are presented. In section 3.4, the experiments and results are presented.

3.2 Constraints for Implicit Calibration Process

3.2.1 Binocular Constraint

Model et al.[11] proposed an optimization procedure with an anatomical constraint to estimate the subject specific parameters implicitly. The proposed binocular constraint assumes that the two visual axes intersect at gaze point. This assumption can be expressed in the following objective function.

$$f(\alpha^L, \beta^L, \alpha^R, \beta^R) = \sum_{i=1}^{i=N} \|G_i^L(\alpha^L, \beta^L) - G_i^L(\alpha^R, \beta^R)\|_2^2 \tag{3.1}$$

The superscripts, L and R on G, α, and β denote the left eye and the right eyes respectively. G_i is the i_{th} gaze point that consists of x and y component relative to the top left corner of the screen. The subscript i denotes the different samples of the gaze. α and β are the subject specific parameters that are described in chapter 2. Exploiting the assumption that two visual axes intersect at gaze point, equation 3.1 finds the α and β parameters that minimizes the distance between the two estimated gaze points. This method directly estimates the eye parameter from the constraint,

---

This chapter previously appeared as: W. Maio and J. Chen and Q. Ji Constraint-based gaze estimation without active calibration. Proc. IEEE Conf. on Automatic Face Gesture Recognition and Workshops (FG) 2011, pp. 627-631.

but it is difficult to achieve accurate results because of the image noise. To alleviate this problem, we propose additional constraints described in the next two sections.

3.2.2 Screen Constraint

Assuming the user is looking at a general area of an object, we can impose the constraint that all of the visual axes intersect at a confined area of the object. This constraint limits the scope of the eye gaze. In our experiment, the screen size is 1280 by 1024 pixels and 360 by 287 mm. The following inequality constraints can be imposed if our assumption is correct.

$$0 < G_{xi}^{L}, G_{xi}^{R} < 1280 \tag{3.2}$$

$$0 < G_{yi}^{L}, G_{yi}^{R} < 1024 \tag{3.3}$$

3.2.3 Eye Parameter Constraint

Similar to many parameters in the human body, a user's eye parameters should fall within a particular range. Using this knowledge, we can construct a range using previously obtained eye parameters from the traditional 9-point calibration process. This simple but powerful constraint improves the optimization process by filtering unreasonable results. Based on an analysis of eye parameters α and β, the following are the ranges of the subject specific parameters.

$$-3.0 \leq \alpha^{L} \leq 1.5 \tag{3.4}$$

$$-3.5 \leq \beta^{L} \leq 1.0 \tag{3.5}$$

$$-2.0 < \alpha^{R} \leq 1.5 \tag{3.6}$$

$$-3.0 \leq \beta^{R} \leq 3.0 \tag{3.7}$$

3.3 Personal Eye Parameter Estimation Process

Given the binocular constraint, the screen constraint and the subject independent parameter range constraint, an constrained optimization problem is formed.

The binocular constraint and our new novel constraints can be expressed in the following equations,

$$s(\alpha^L, \beta^L, \alpha^R, \beta^R) = \begin{bmatrix} G_{x_i}^{L,R} - 1280 \\ -G_{x_i}^{L,R} \\ G_{y_i}^{L,R} - 1024 \\ -G_{y_i}^{L,R} \end{bmatrix} \tag{3.8}$$

$$p(\alpha^L, \beta^L, \alpha^R, \beta^R) = \begin{bmatrix} -3.5 - \alpha^L \\ \alpha^L - 1.5 \\ -3.5 - \beta^L \\ \beta^L - 1.0 \\ -2.0 - \alpha^R \\ \alpha^R - 1.5 \\ -3.0 - \beta^R \\ \beta^R - 3.0 \end{bmatrix} \tag{3.9}$$

$$\begin{aligned} &\min_{\alpha^L, \beta^L, \alpha^R, \beta^R} f(\alpha^L, \beta^L, \alpha^R, \beta^R) \\ &\textit{subject to } s_j(\alpha^L, \beta^L, \alpha^R, \beta^R) \leq 0 \quad j = 1, \ldots 4 \\ &p_k(\alpha^L, \beta^L, \alpha^R, \beta^R) \leq 0 \quad k = 1, \ldots 8 \end{aligned} \tag{3.10}$$

where (3.8) is the screen constraint using the parameters in (3.2) and (3.3), and (3.9) is the subject independent parameter range constraint using parameters in (3.4),(3.5),(3.6),(3.7). The initialization used for this constrained non-linear optimization problem is the average subject parameters. It can also be obtained from anthropological statistics. The following is the initial point for the optimization.

$$\alpha^L = -0.1528^\circ,\ \beta^L = -0.9468^\circ,\ \alpha^R = -0.3995^\circ,\ \beta^R = -0.5832^\circ \tag{3.11}$$

This problem can be solved using quadratic programming [2].

3.4 Experiments and Results

We used the traditional 9-point calibration data set to validate our implicit subject specific parameter estimation. To compare our method, we also compared with Model's method with the binocular constraint only [11].

Table 3.1: Subject Specific Parameter Estimation Result with Eye Parameter Range Constraint

Subject	Subject-Specific Parameter							
	9-Point Calibration (°)				Proposed Method (°)			
	α^L	β^L	α^R	β^R	α^L	β^L	α^R	β^R
1	1.3	-1.2	-0.2	-1.5	1.5	-3.0	0.0	-2.7
2	-3.0	3.5	1.3	-3.0	-3.0	-2.8	1.5	-3.0
3	1.0	0.9	-1.9	-0.6	-1.5	-3.0	-0.6	-0.4
4	0.2	0.0	-0.8	2.9	-1.5	-3.0	-2.0	-0.4

Table 3.1 shows the results of the estimated eye parameters using the proposed method with only the eye parameter range constraint[3] and the 9-point method. Due to the image noise in the gaze estimation system, for some subjects, the parameters do not quite converge to the results for 9-point calibration method. However, when compared to other methods in Table 3.2, the improvement is significant.

[3]The result using the proposed method with only the eye parameter range constraint is presented here because the eye parameter range constraint is a stricter constraint than the screen constraint for all the estimated gaze point for all tested subjects.

Table 3.2: Gaze Angle Deviation Using Different Methods

Subject	Angle Deviation from Calibration Points							
	9P (°)		E2 (°)		E2P (°)		E2S (°)	
	G^L	G^R	G^L	G^R	G^L	G^R	G^L	G^R
1	2.6	2.4	12.0	12.0	2.9	2.4	11.0	8.9
2	2.8	2.4	8.2	3.4	2.9	2.7	8.2	3.4
3	2.1	3.9	5.6	22.0	4.0	4.4	6.5	8.6
4	3.8	3.6	7.9	19.0	5.6	5.5	6.3	5.4
Average	2.8	3.1	8.4	14.1	3.9	3.8	8.0	6.6

Table 3.2 summarizes the deviation of the gaze estimation from the calibration points. The 9P column is the result of the 9-point calibration. The E2 column is the result of the Model's method in [11] applied on a conventional screen.[4] The E2P column is the result with the subject independent eye parameter range constraint. E2S column is the result with the screen constraint. The result is in terms of the accuracy of the estimated gaze angles. In all the experiments, the subject sat 500 mm away from the screen. It is clear that the eye parameter range constraint can effectively reduce the estimate error, while the screen constraint can only marginally improve the estimation error as compared with the Model's method.

We tried different combinations of constraints and found that subject independent parameter eye range constraint produced results that were the most comparable to the 9-point calibration process. We also found that the subject independent eye parameter range constraint is a stricter constraint than the screen constraint. When the optical axis already intersects with the screen, the screen constraint does not affect the optimization. Table 3.3 shows the deviation between the estimated gaze and actual gaze at each of the evenly distributed calibration points starting with top left calibration point in the first row and first column of 16 mm deviation of the left eye using the traditional 9-point calibration method for subject 1.

[4] In [11], the optimization criterion works reasonably with a pyramid surface. Model's method applied on a conventional display is expected to have large error.

Table 3.3: Estimated Gaze Deviation from Calibration Points

Subject 1	Deviation from Calibration Points					
	9-Point (mm)			Our Method (mm)		
Left Eye	16.6	27.7	1.8	16.0	29.4	10.4
	19.1	28.4	31.1	21.7	34.1	27.8
	25.5	24.8	26.0	28.2	24.4	25.4
Right Eye	18.0	31.6	13.5	18.2	30.0	13.3
	28.9	27.2	16.8	27.6	26.1	16.7
	14.8	19.4	17.0	14.4	21.0	18.1

Figure 3.1 presents the scan pattern of the 9-point calibration process and our method.

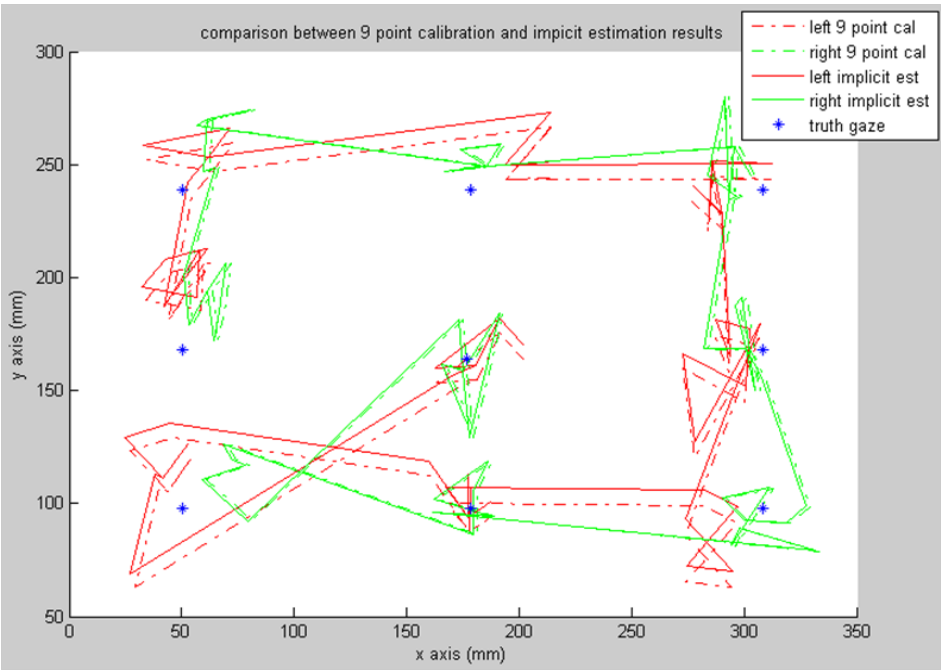

Figure 3.1: The gaze estimation result of subject 1

The green and red are the left gaze and right gaze. The dash-dot line is the gaze using the 9-point calibration parameter and the solid line is the gaze using the implicit parameter estimation. The blue star is the ground truth. The solid line is

the estimated gaze using the parameter obtained from our method and the dash-dot line is the estimated gaze using the parameter obtained from the 9-point calibration method. From figure 3.1, we can conclude that the implicit parameter estimation method produces a scan pattern that closely follows the 9-point calibration result.

The reason for the poor performance of the binocular constraint only is revealed by analyzing the optimization progress in figures 3.2 and 3.3. The effects of adding the two additional constraint is presented in figures 3.4 and 3.5. The first plot is the result of the right and left gaze mean square error deviation at each of the optimization iterations. The second plot is the evaluation of equation (3.1) at each of the iterations. Note that the result from the binocular constraint-only method initially minimizes the objective function and reduces the mean square error, but after 10 iterations, due to the image noise the deviation between the actual gaze and estimated gaze increases. This shows the method's instability.

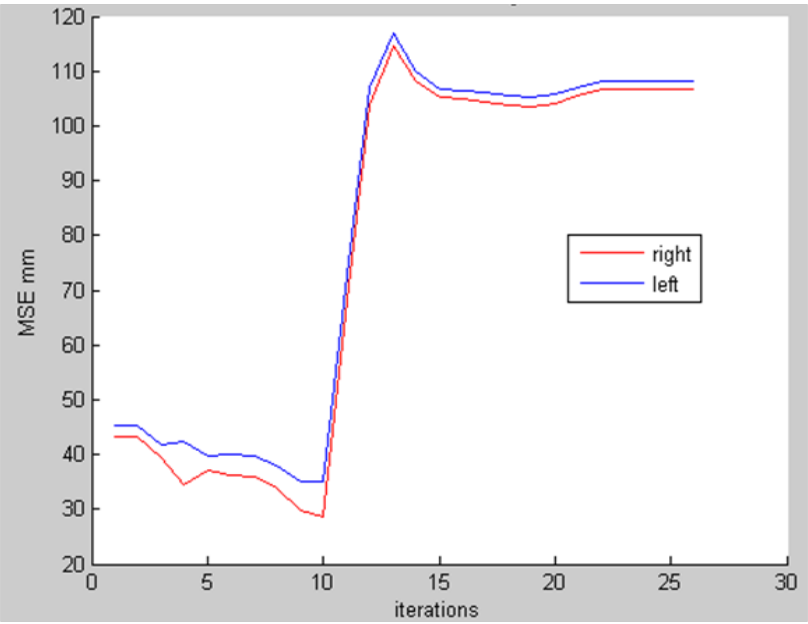

Figure 3.2: Mean square error of the left and right eye gaze estimation in each optimization iteration using only the binocular constraint

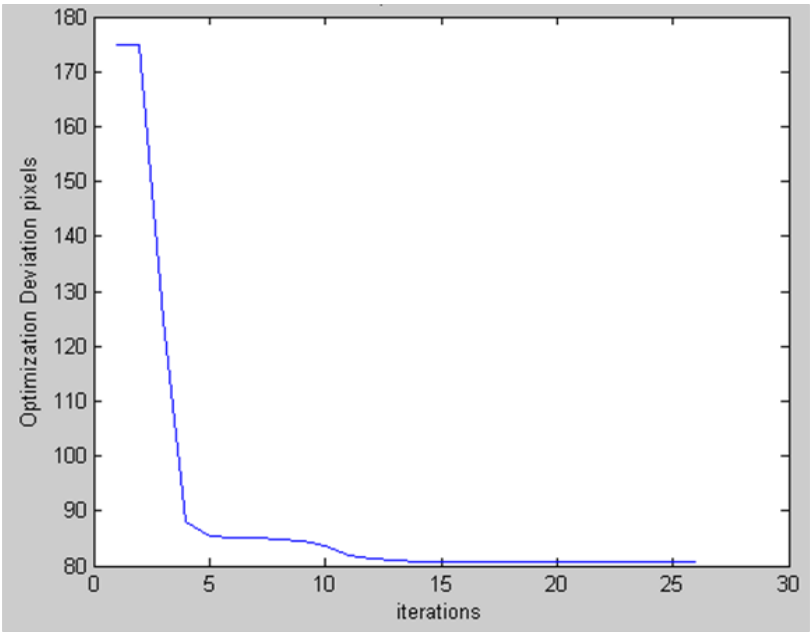

Figure 3.3: Objective function evaluation in each iteration using the binocular constraint only

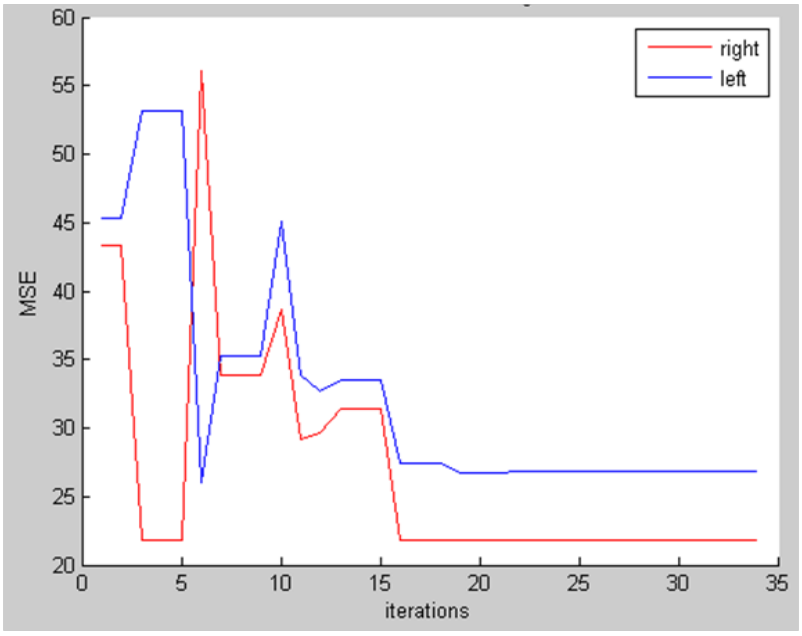

Figure 3.4: Mean square error of the left and right eye gaze estimation in each optimization iteration using our method

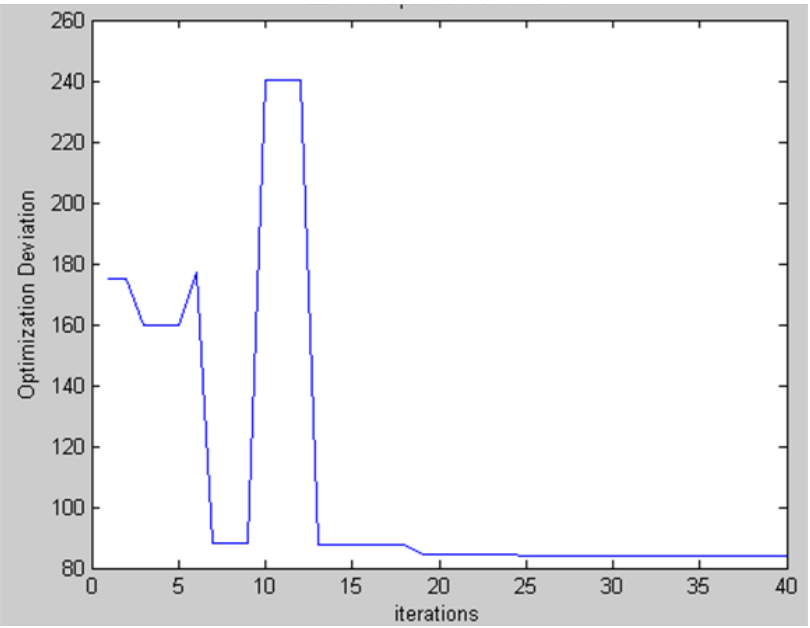

Figure 3.5: Objective function evaluation in each iteration using our method

Adding on the constraints to the objective function, we observe a decrease in both the MSE in mm and the objective function as it settles down around 30 iterations. When the optimization is stable with constraint, the result is comparable to the 9-Point calibration algorithm.

3.5 Chapter Conclusion

We have presented a constraint-based gaze-estimation without explicit calibration process. With this technique, the system automatically calibrates the user while the user looks at the screen freely. Compared with similar existing methods, our method is simple and effective. It can lead to smoother interaction with eye-gaze technology. In the future, we intend to further validate the method with additional subjects and under different operating conditions. In addition, we will identify additional constraints to further improve the accuracy and robustness of this approach.

CHAPTER 4
Calibration-free Gaze Tracking via Eye Measurement Matrix Factorization

4.1 Introduction

In this chapter, we build a framework based on the assumption that the difference between the optical axis and the visual axis is a constant angle deviation represented by a subject-specific rotation matrix that is only a function of the subject specific parameters α and β. Compared to the stereo eye gaze tracking, this approach uses a monocular camera, which allows a larger head movements. After collecting several observations, we formulate a measurement matrix with the optical axes ($\vec{op}$), and factorizes the matrix via singular value decomposition (SVD). The subject-specific parameter is recovered from the result of the factorization. The assumption can be described by the following equation,

$$\vec{op}(\theta, \phi) = \vec{vis}(\theta, \phi, \alpha, \beta)R(\alpha, \beta) \tag{4.1}$$

where $\vec{op}$ is the optical axis, $\vec{vis}$ is the visual axis, and R is the subject-specific rotation matrix that we want to estimate from using $\vec{op}$ only.

4.2 Personal Eye Parameter Rotation Matrix Analysis

Intuitively, the assumption of equation (4.1) should be true, since the angle deviation between the optical axis and the visual axis is fixed. To verify the assumption that there is a rotation matrix that describes the constant angle deviation from visual axis and optical axis as in equation (4.1), the dot product between $\vec{op}$

and $\vec{vis}$ is evaluated.

$$
\begin{aligned}
dot(\vec{op}, \vec{vis}) &= \begin{bmatrix} \cos(\phi)\sin(\theta) \\ \sin(\phi) \\ -\cos(\phi)\cos(\theta) \end{bmatrix} \cdot \begin{bmatrix} \cos(\phi+\beta)\sin(\theta+\alpha) \\ \sin(\phi+\beta) \\ -\cos(\phi+\beta)\cos(\theta+\alpha) \end{bmatrix} \\
&= \cos(\phi)\sin(\theta)\cos(\phi+\beta)\sin(\theta+\alpha) + \sin(\phi)\sin(\phi+\beta) \\
&+ \cos(\phi)\cos(\theta)\cos(\phi+\beta)\cos(\theta+\alpha) \\
&= \cos(\phi)\cos(\phi+\beta)(\cos(\theta)\cos(\theta+\alpha) + \sin(\theta)\sin(\theta+\alpha)) + \sin(\phi)\sin(\phi+\beta) \\
&= \cos(\phi)\cos(\phi+\beta)\cos(\alpha) + \sin(\phi)\sin(\phi+\beta)
\end{aligned}
\tag{4.2}
$$

From equation (4.2), we can see that the view direction parameter ϕ is still present in equation (4.2). Therefore, directly using the trigonometric representation of the optical and visual axes is not feasible. To solve this problem, the matrix representation of the $\vec{op}$ and $\vec{vis}$ is derived to decouple the rotation angles and to better understand the relationship between the optical axis and visual axis.

4.3 Matrix Representation

In this section, the matrix representation of the relationship between $\vec{op}$ and $\vec{vis}$ is presented in section 4.3.1. In section 4.3.2, the matrices that relates the optical axis to visual axis are presented.

4.3.1 Optical Axis and Visual Axis Rotation Matrices Representation

The trigonometric representation of $\vec{op}$ amd $\vec{vis}$ from equation (2.1) and (2.2) can be represented by rotation matrices resulted from rotating an initial axis. Both the orientation of the visual axis and optical axis are modeled as rotation angles from the -z axis as shown in figure 2.2. The initial axis is set to $-z$ direction ($\begin{bmatrix} 0 \\ 0 \\ -1 \end{bmatrix}$), which is also the axis when all of the parameters of equation (2.1) and (2.2) are set

to zero. Then, the matrix representation of the axes are the following two equations[5]

$$\vec{op} = \begin{bmatrix} \cos(\phi)\sin(\theta) \\ \sin(\phi) \\ -\cos(\phi)\cos(\theta) \end{bmatrix} = R_y(-\theta)R_x(\phi)\begin{pmatrix} 0 \\ 0 \\ -1 \end{pmatrix} \tag{4.3}$$

$$\begin{aligned} \vec{vis} &= \begin{bmatrix} \cos(\phi+\beta)\sin(\theta+\alpha) \\ \sin(\phi+\beta) \\ -\cos(\phi+\beta)\cos(\theta+\alpha) \end{bmatrix} = R_y(-\theta-\alpha)R_x(\phi+\beta)\begin{pmatrix} 0 \\ 0 \\ -1 \end{pmatrix} \\ &= R_y(-\theta)R_y(-\alpha)R_x(\beta)R_x(\phi)\begin{pmatrix} 0 \\ 0 \\ -1 \end{pmatrix} \end{aligned} \tag{4.4}$$

In equation (4.3), the optical axis is described by first rotating -z as illustrated in figure 2.2 about the y-axis by $-\theta$ degrees, followed by a rotation about the x-axis by ϕ degrees. Similarly, the visual axis is described by equation (4.4) with subject specific parameters added on to the view angles.

4.3.2 Relationship Between Optical Axis and Visual Axis

Working towards finding the subject specific parameter from the optical axes only, the matrices that relates the optical axis to the visual axis are found. First the common entry of the two equations are found in equation (4.3) and (4.4),

$$R_y(\theta)\vec{op} = R_x(-\beta)R_y(\alpha)R_y(\theta)\vec{vis} = R_x(\phi)\begin{bmatrix} 0 \\ 0 \\ -1 \end{bmatrix} \tag{4.5}$$

Manipulating (4.5), we can find the matrices that relate the two axes together.[6]

$$\vec{op} = R_y(-\theta)R_x(-\beta)R_y(\alpha)R_y(\theta)\vec{vis} \tag{4.6}$$

[5]Please refer to Appendix A for the derivation

[6]Note that rotation matrices with common rotation axis are commutative. Please refer to Appendix B.1. Also the transpose of the rotation matrices it the same as rotating in the negative direction. Please refer to Appendix B.2.

Equation (4.6) is the key equation in the decomposition approach to recover subject-specific parameters.

4.4 Personal Eye Parameters from Singular Value Decomposition

Traditionally, the subject specific parameters, α and β, are estimated via a calibration process that uses calibration points, which requires active user cooperation. In this study, the subject specific-parameters are represented by rotation matrices $R_y(\alpha)$ and $R_x(\beta)$, which are estimated from factorizing the matrix constructed from bundles of optical axes. This way, the eye-tracking system is able to track the user's gaze accurately without any user cooperation. From (4.6), we can reorganize the matrices to separate the matrices that are only a function of the subject specific parameters, $R_y(\alpha)$ and $R_x(\beta)$ from the rest of the equations.

$$R_y(\theta)\vec{op} = R_x(-\beta)R_y(\alpha)R_y(\theta)\vec{vis} \tag{4.7}$$

Note that $\vec{op}$ is a function of θ and ϕ, and $\vec{vis}$ is a function of θ, ϕ, α, and β. Taking the transpose of equation (4.7), we have the following equation.[7]

$$\vec{op}^{\,t}R_y(-\theta) = \vec{vis}^{\,t}R_y(-\theta)R_y(-\alpha)R_x(\beta) \tag{4.8}$$

In equation (4.8) the $R_y(-\alpha)R_x(\beta)$ rotation matrices, which is only dependent on the subject parameters, are isolated from the other parameters. Then, the implicit calibration process becomes estimating $R_y(-\alpha)R_x(\beta)$ from the observable variables $\vec{op}^{\,t}R_y(-\theta)$. Multiple equations of (4.8) with different θ and ϕ parameters will be

[7]Note that the transpose of the rotation matrices is equivalent of rotating in the oppose direction please refer to Appendix B.2.

combined to form a measurement matrix for factorization.

$$\begin{bmatrix} \vec{op}_1^{\,t} R_y(-\theta_1) \\ \vec{op}_2^{\,t} R_y(-\theta_2) \\ \vdots \\ \vec{op}_N^{\,t} R_y(-\theta_n) \end{bmatrix} = \begin{bmatrix} \vec{vis}_1^{\,t} R_y(-\theta_1) \\ \vec{vis}_2^{\,t} R_y(-\theta_2) \\ \vdots \\ \vec{vis}_N^{\,t} R_y(-\theta_n) \end{bmatrix} R_y(-\alpha) R_x(\beta) \tag{4.9}$$

In equation (4.9), all of the unknown parameters are on the right side of the equation while the parameters on the left side of the equation are all known. Representing the 3 different matrices by symbols, we have the following important equation[8].

$$A_{n\times 3} = B_{n\times 3} R_{3\times 3} \tag{4.10}$$

where $A_{n\times 3} = \begin{bmatrix} \vec{op}_1^{\,t} R_y(-\theta_1) \\ \vec{op}_2^{\,t} R_y(-\theta_2) \\ \vdots \\ \vec{op}_n^{\,t} R_y(-\theta_n) \end{bmatrix}$; $B_{n\times 3} = \begin{bmatrix} \vec{vis}_1^{\,t} R_y(-\theta_1) \\ \vec{vis}_2^{\,t} R_y(-\theta_2) \\ \vdots \\ \vec{vis}_N^{\,t} R_y(-\theta_n) \end{bmatrix}$; $R_{3\times 3} = R_y(-\alpha) R_x(\beta)$, the 3 by 3 rotation matrix with only subject specific parameters. A is called the measurement matrix. Equation (4.10) is the key equation in this approach through which we investigate the feasibility of recovering R via the measurement matrix A.

4.5 Analyzing the Rank of $A = BR$

Before discussing solutions to recover R from A, the rank of A, B, R matrices are analyzed to better understand the structure of each of the matrices.

4.5.1 Rank of A

To analyze the rank of A, the matrix representation of a single row of A is presented to provide insights into the rank of A. From equation (4.3), we have

$$\vec{op}^{\,t} R_y(-\theta) = \begin{bmatrix} 0 & 0 & -1 \end{bmatrix} R_x(-\phi) R_y(\theta) R_y(-\theta) = \begin{bmatrix} 0 & \sin(\phi) & -\cos(\phi) \end{bmatrix} \tag{4.11}$$

[8]Please refer to Appendix C for the verification of the equation derivation.

From equation (4.11), the rotation matrix $R_y(-\theta)$ cancels out the rotation matrix $R_y(\theta)$, yielding the right side of equation (4.11). The property of A matrix makes each of the first columns of row of A be 0. The rest of the columns are sin and cos functions of ϕ, which are linearly independent, but nonlinearly related. Consequently, the rank of A is hence 2.

4.5.2 Rank of B

To analyze the rank of B, the rotation representation and a single row of B is presented to provide insights into the rank of B. Again, from equation (4.4), we have

$$\begin{aligned} B_i = \vec{vis}^{\,t} R_y(-\theta_i) &= \begin{bmatrix} 0 & 0 & -1 \end{bmatrix} R_x(-\phi_i) R_x(-\beta) R_y(\alpha) R_y(\theta_i) R_y(-\theta_i) \\ &= \begin{bmatrix} \sin(\alpha)\cos(\phi_i+\beta) & \sin(\phi_i+\beta) & -\cos(\alpha)\cos(\phi_i+\beta) \end{bmatrix} \end{aligned} \tag{4.12}$$

From the structure of equation (4.12), no feature is apparent to determine the rank. Therefore, the determinant of a sub-matrix of B is taken to investigate whether the sub-matrix is rank-deficient. If the determinant is 0, the sub-matrix of B contains rows or columns that are linearly dependent of each other, which makes sub-matrix of B rank-deficient.

$$\det(B_{1,2,3}) = \det \begin{bmatrix} \sin(\alpha)\cos(\phi_1+\beta) & \sin(\phi_1+\beta) & -\cos(\alpha)\cos(\phi_1+\beta) \\ \sin(\alpha)\cos(\phi_2+\beta) & \sin(\phi_2+\beta) & -\cos(\alpha)\cos(\phi_2+\beta) \\ \sin(\alpha)\cos(\phi_3+\beta) & \sin(\phi_3+\beta) & -\cos(\alpha)\cos(\phi_3+\beta) \end{bmatrix} = 0 \tag{4.13}$$

From equation (4.13)[9], we can see that the determinant of the sub-matrix of B is indeed 0, thus we have evidence that suggests matrix B is not full rank. Observing the trigonometry function and the parameters of equation (4.13), the first and third column of B have the same $\cos(\phi_i + \beta)$ multiplied by a different constant. This makes the first and third column of B linearly dependent, which also suggests that the rank of B is 2.

[9]Further theoretical proof is needed to establish the fact that the $Rank(B) = 2$. Please refer to Appendix D.1 for the equation derivation.

4.5.3 Rank of R

To analyze the rank of R, the explicit trig-function is presented.

$$\begin{aligned} R = R_y(-\alpha)R_x(\beta) &= \begin{bmatrix} \cos(\alpha) & 0 & -\sin(\alpha) \\ 0 & 1 & 0 \\ \sin(\alpha) & 0 & \cos(\alpha) \end{bmatrix} \begin{bmatrix} 1 & 0 & 0 \\ 0 & \cos(\beta) & -\sin(\beta) \\ 0 & \sin(\beta) & \cos(\beta) \end{bmatrix} \\ &= \begin{bmatrix} \cos(\alpha) & -\sin(\alpha)\sin(\beta) & -\sin(\alpha)\cos(\beta) \\ 0 & \cos(\beta) & -\sin(\beta) \\ \sin(\alpha) & \cos(\alpha)\sin(\beta) & \cos(\alpha)\cos(\beta) \end{bmatrix} \end{aligned} \tag{4.14}$$

From the structure of equation (4.14), no obvious structure is apparent to determine the rank. Therefore, the determinant of the R matrix is taken to investigate whether the R matrix is rank-deficient.

$$det(R) = \begin{bmatrix} \cos(\alpha) & -\sin(\alpha)\sin(\beta) & -\sin(\alpha)\cos(\beta) \\ 0 & \cos(\beta) & -\sin(\beta) \\ \sin(\alpha) & \cos(\alpha)\sin(\beta) & \cos(\alpha)\cos(\beta) \end{bmatrix} = 1 \tag{4.15}$$

From equation (4.15)[10], we can see that the determinant of R is 1, which makes R invertible and full rank. This result is expected, since a rotation matrix is always invertible, and R comprises of 2 rotation matrices; the multiplication of rotation matrices produces another rotation matrices. If the matrix is invertible, then the rank of the matrix equals the size of the matrix. Thus, the rank of R is 3.

4.6 Solving for the Personal Eye Parameter Rotation Matrix

In section 4.6.1, the relationship between the measurement matrix and the subject-specific rotation matrix is presented along with one of the solutions. In section 4.6.2 and 4.6.3, the SVD of A is analyzed analytically and empirically. In section 4.6.4, all analysis in this section will be combined.

[10]Please refer to appendix D.2 for the equation derivation.

4.6.1 Personal Eye Parameter from SVD of Measurement Matrix

First, we perform a SVD on the measurement matrix A as follows.

$$A = UDV^t \tag{4.16}$$

Comparing equation (4.10) with equation (4.16), we have one possible solution for B and R as $B = UD$ and $R = V^t$. Since $BR = B\hat{R}\hat{R}^tR$, the solution to R must be up to a rotation matrix $\hat{R}$. Let's denote the rotation matrix as $\hat{R}$, and insert $\hat{R}\hat{R}^t$ into equation (4.16) between UD and V^t.

$$A = UD\hat{R}\hat{R}^tV^t \tag{4.17}$$

Equation (4.17) is still the same as equation (4.16), since the product of $\hat{R}$ and $\hat{R}^t$ is the identity matrix. To simplify the equation, let's denote UD as $\hat{B}$. The rotation matrix $\hat{R}$ should relate the factorization of A to the ground truth variables. Thus, we have the following two equations,

$$B = \hat{B}\hat{R} \tag{4.18}$$

$$R = \hat{R}^tV^t \tag{4.19}$$

where $\hat{B}$ and V^t are both known from equation (4.16). Our goal is now to estimate $\hat{R}$, based on which we can recover R and B.

4.6.2 SVD Structure Analysis

To better understand equation (4.16), the SVD of measurement matrix A is analyzed in this section. The columns of U and rows of V^t from equation (4.16) correspond to the eigenvectors of AA^t and eigenvectors of A^tA. The matrix A^tA is examined to simplify the analysis, since the size of A^tA is 3 by 3. The eigenvalues of A^tA is derived in this section, which will be used in later section to solve for the eigenvectors of A^tA, which is also the rows of V^t. The product of A^tA is given by

the following equation.

$$A^tA = \begin{bmatrix} 0 & 0 & 0 & \cdots & 0 \\ \sin(\phi_1) & \sin(\phi_2) & \sin(\phi_3) & \cdots & \sin(\phi_N) \\ -\cos(\phi_1) & -\cos(\phi_2) & -\cos(\phi_3) & \cdots & -\cos(\phi_N) \end{bmatrix} \begin{bmatrix} 0 & \sin(\phi_1) & -\cos(\phi_1) \\ 0 & \sin(\phi_2) & -\cos(\phi_2) \\ 0 & \sin(\phi_3) & -\cos(\phi_3) \\ \vdots & \vdots & \vdots \\ 0 & \sin(\phi_N) & -\cos(\phi_N) \end{bmatrix}$$

$$= \begin{bmatrix} 0 & 0 & 0 \\ 0 & \sum_{i=1}^{i=N} \sin^2(\phi_i) & -\frac{1}{2}\sum_{i=1}^{i=N} \sin(2\phi_i) \\ 0 & -\frac{1}{2}\sum_{i=1}^{i=N} \sin(2\phi_i) & \sum_{i=1}^{i=N} \cos^2(\phi_i) \end{bmatrix}$$

$$= \begin{bmatrix} 0 & 0 & 0 \\ 0 & \frac{1}{2}(N - \sum_{i=1}^{i=N} \cos(2\phi_i)) & -\frac{1}{2}\sum_{i=1}^{i=N} \sin(2\phi_i) \\ 0 & -\frac{1}{2}\sum_{i=1}^{i=N} \sin(2\phi_i) & \frac{1}{2}(N + \sum_{i=1}^{i=N} \cos(2\phi_i)) \end{bmatrix} \tag{4.20}$$

To solve for the eigenvalues of A^tA, we find the λ_{eig} in the following equation,

$$det(A^tA - \lambda_{eig}I) = 0$$

$$= det \begin{bmatrix} -\lambda_{eig} & 0 & 0 \\ 0 & \frac{1}{2}(N - \sum_{i=1}^{i=N} \cos(2\phi_i)) - \lambda_{eig} & -\frac{1}{2}\sum_{i=1}^{i=N} \sin(2\phi_i) \\ 0 & -\frac{1}{2}\sum_{i=1}^{i=N} \sin(2\phi_i) & \frac{1}{2}(N + \sum_{i=1}^{i=N} \cos(2\phi_i)) - \lambda_{eig} \end{bmatrix}$$

$$= -\lambda_{eig}(\frac{1}{4}((N + \sum_{i=1}^{i=N} \cos(2\phi_i))(N - \sum_{i=1}^{i=N} \cos(2\phi_i)) - \lambda_{eig}N + \lambda_{eig}^2)$$

$$- (\frac{1}{2}\sum_{i=1}^{i=N} \sin(2\phi_i))^2)$$

$$= -\lambda_{eig}(\frac{1}{4}N^2 - \lambda_{eig}N + \lambda_{eig}^2 - \frac{1}{4}(\sum_{i=1}^{i=N} \cos(2\phi_i))^2 + (\sum_{i=1}^{i=N} \sin(2\phi_i))^2)$$

$$= -\lambda_{eig}((\frac{1}{2}N - \lambda_{eig})^2 - \frac{1}{4}((\sum_{i=1}^{i=N} \cos(2\phi_i))^2 + (\sum_{i=1}^{i=N} \sin(2\phi_i))^2)) \tag{4.21}$$

From equation (4.21), the trivial solution for λ_{eig} is 0. The non-trivial solution is given by the following equation,

$$
\begin{aligned}
(\frac{1}{2}N - \lambda_{eig})^2 - \frac{1}{4}((\sum_{i=1}^{i=N}\cos(2\phi_i))^2 + (\sum_{i=1}^{i=N}\sin(2\phi_i))^2) &= 0 \\
\frac{1}{2}N - \lambda_{eig} = \pm\frac{1}{2}\sqrt{((\sum_{i=1}^{i=N}\cos(2\phi_i))^2 + (\sum_{i=1}^{i=N}\sin(2\phi_i))^2)} & \\
\lambda_{eig} = \frac{1}{2}N \pm \frac{1}{2}\sqrt{((\sum_{i=1}^{i=N}\cos(2\phi_i))^2 + (\sum_{i=1}^{i=N}\sin(2\phi_i))^2)} &
\end{aligned}
\tag{4.22}
$$

Thus, the eigenvalues of A^tA, which corresponds to the diagonal entries of matrix D in SVD, is,

$$
\lambda_{eig} = 0, \frac{1}{2}N \pm \frac{1}{2}\sqrt{((\sum_{i=1}^{i=N}\cos(2\phi_i))^2 + (\sum_{i=1}^{i=N}\sin(2\phi_i))^2)} \tag{4.23}
$$

4.6.3 SVD Structure from Data

In this section, to further study the factorization of the measurement matrix, the solution of the SVD is analyzed. The complicated functions in equation (4.20) prevents us from finding the eigenvectors of A^tA, which corresponds to rows of V^t in equation (4.16). To resolve this, we numerically experimented with equation (4.16) to study the structure of the equation. From the numerical experiment of equation (4.16), there is a constant angle parameter η parameter that can be identified. The matrices UD and V^t can be parametrized by this η parameter along with the ϕ parameter from the measurement matrix A. We identified that the V^t matrix is only a function of η.

$$
V^t = \begin{bmatrix} 0 & \pm\sin(\eta) & \pm\cos(\eta) \\ 0 & \pm\cos(\eta) & \pm\sin(\eta) \\ \pm 1 & 0 & 0 \end{bmatrix} \tag{4.24}
$$

For matrices UD, the η parameter is observed with the ϕ parameter from the measurement matrix.[11]

$$UD = \begin{bmatrix} \pm\cos(\phi_i \pm \eta) & \pm\sin(\phi_i \pm \eta) & 0 \end{bmatrix} \tag{4.25}$$

Using the identified structure from this section and the eigenvalues of A^tA from equation (4.23), eigenvectors of A^tA (rows of V^t) can be verified by finding the solution of η. Please refer to Appendix F for the analysis.

4.6.4 One Possible Factorization

We derived $\hat{R}$ that maps R to V^t as in equation (4.19). Manipulating equation (4.19), we have the following equation,

$$\hat{R}R = V^t \tag{4.26}$$

In this section, the $\hat{R}$ is derived using the analysis of the SVD of A. From numerical simulations of sections 4.6.3, the structure of V^t has the following structure,

$$V^t = \begin{bmatrix} 0 & \pm\sin(\eta) & \pm\cos(\eta) \\ 0 & \pm\cos(\eta) & \pm\sin(\eta) \\ \pm 1 & 0 & 0 \end{bmatrix} \tag{4.27}$$

To relate R to V^t, we need to find $\hat{R}$ such that the entries of $\hat{R}R$ match the 0 and 1 entries in V^t

$$R = \begin{bmatrix} \cos(\alpha) & -\sin(\alpha)\sin(\beta) & -\sin(\alpha)\cos(\beta) \\ 0 & \cos(\beta) & -\sin(\beta) \\ \sin(\alpha) & \cos(\alpha)\sin(\beta) & \cos(\alpha)\cos(\beta) \end{bmatrix} \tag{4.28}$$

Hence, the following entries of V^t must be zero, V^t_{11}, V^t_{21}, V^t_{32}, V^t_{33}, and the V^t_{13} must be 1. The rotation matrix $\hat{R}$ from equation (4.19) can be constructed using the matching structure. Given V^t_{13} from equation (4.27), the last row of $\hat{R}$ must be the

[11] Please refer to Appendix E for the full combination of the structure.

following to produce the zero and one entries in V^t

$$\begin{bmatrix}\cos(\alpha) & 0 & \sin(\alpha)\end{bmatrix} \tag{4.29}$$

Then, the remaining rows of $\hat{R}^t$ must be orthogonal to equation (4.29) and orthogonal to each other, choosing an arbitrarily orthogonal vector, we have the following matrix, as one of the possible solutions for $\hat{R}$

$$\hat{R} = \begin{bmatrix} 0 & 1 & 0 \\ \sin(\alpha) & 0 & -\cos(\alpha) \\ \cos(\alpha) & 0 & \sin(\alpha) \end{bmatrix} \tag{4.30}$$

Applying the $\hat{R}$ to R, the following result is yielded.

$$\begin{bmatrix} 0 & 1 & 0 \\ \sin(\alpha) & 0 & -\cos(\alpha) \\ \cos(\alpha) & 0 & \sin(\alpha) \end{bmatrix} \begin{bmatrix} \cos(\alpha) & -\sin(\alpha)\sin(\beta) & -\sin(\alpha)\cos(\beta) \\ 0 & \cos(\beta) & -\sin(\beta) \\ \sin(\alpha) & \cos(\alpha)\sin(\beta) & \cos(\alpha)\cos(\beta) \end{bmatrix} = \begin{bmatrix} 0 & \cos(\beta) & -\sin(\beta) \\ 0 & \sin(\beta) & \cos(\beta) \\ 1 & 0 & 0 \end{bmatrix} \tag{4.31}$$

From equation (4.31), it is possible that the angle η parametrized in V^t is equal to the β parameter, and β can therefore be solved from V^t, i.e,

$$\cos(\beta) = V^t(1,2) \tag{4.32}$$

$$\sin(\beta) = V^t(2,2) \tag{4.33}$$

From this study, we derived a rotation matrix $\hat{R}$ that can lead to the solution of β. Another method is needed to derive the matrix that can lead to the solution of α.

4.7 Experiments and Results

In this section, the data used for the experiment are presented in section 4.7.1. Then, the result of the SVD of the measurement matrix is presented in section 4.7.2.

4.7.1 Synthetic Data

To validate the equations, we use synthetic data generated from different users as shown in 4.7.1

Table 4.1: Sample Subject Specific Parameters

Users	α	β
User 1	1.276	-0.312
User 2	2.708	-0.762
User 3	1.273	-3.017
User 4	-0.809	0.163
User 5	-1.863	0.968
User 6	-0.193	1.274
Average	0.3987	-0.2810

Using the parameter reflective of the true value, the average parameter of six subjects is set for the subject specific parameter ($\alpha = 0.3987$ $\beta = -0.2810$). In this experiment, to represent the most general case, the optical axis is generated from a distribution that is reflective of a realistic data. The range of the angles are $-41.1451 < \phi < -20.0852$ and $-5.2709 < \theta < 30.1427$. 10 samples of optical axis are generated synthetically. Table 4.2, 4.3, 4.4, and 4.5 are the numerical values of the synthetic data.

Table 4.2: ϕ and θ Data Set

	1	2	3	4	5	6	7	8	9	10
ϕ	-37.82	-20.70	-20.98	-30.92	-24.29	-38.15	-32.26	-21.86	-24.46	-20.93
θ	23.58	26.80	-0.77	27.07	17.12	-1.81	4.59	14.09	28.63	28.89

Table 4.3: $\phi + \beta$ and $\theta + \alpha$ Data Set

	1	2	3	4	5	6	7	8	9	10
$\phi + \beta$	-38.10	-20.98	-21.26	-31.20	-24.57	-38.43	-32.54	-22.14	-24.74	-21.21
$\theta + \alpha$	23.98	27.20	-0.37	27.47	17.52	-1.41	4.99	14.49	29.03	29.29

Table 4.4: $\vec{op}$ Data Set

	1	2	3	4	5	6	7	8	9	10
x	0.316	0.421	-0.012	0.390	0.268	-0.024	0.067	0.226	0.436	0.451
y	-0.613	-0.354	-0.358	-0.514	-0.411	-0.618	-0.534	-0.372	-0.414	-0.357
z	-0.723	-0.834	-0.933	-0.763	-0.871	-0.785	-0.842	-0.900	-0.798	-0.817

Table 4.5: $\vec{vis}$ Data Set

	1	2	3	4	5	6	7	8	9	10
x	0.319	0.426	-0.006	0.394	0.273	-0.019	0.073	0.231	0.440	0.456
y	-0.617	-0.358	-0.362	-0.518	-0.415	-0.621	-0.537	-0.376	-0.418	-0.361
z	-0.718	-0.830	-0.931	-0.758	-0.867	-0.783	-0.839	-0.896	-0.794	-0.813

4.7.2 A,B,R Matrices

4.7.2.1 Measurement Matrix, A

The following is the result of measurement matrix A with each row equal to $op_i^t(\theta_i, \phi_i)R_y(-\theta_i)$ and $\begin{bmatrix} 0 & \sin(\phi_i) & -\cos(\phi_i) \end{bmatrix}$ using parameter from section 4.7.1

$$A = \begin{bmatrix} 0.000 & -0.613 & -0.790 \\ 0.000 & -0.354 & -0.935 \\ 0.000 & -0.358 & -0.934 \\ 0.000 & -0.514 & -0.858 \\ 0.000 & -0.411 & -0.911 \\ 0.000 & -0.618 & -0.786 \\ 0.000 & -0.534 & -0.846 \\ 0.000 & -0.372 & -0.928 \\ 0.000 & -0.414 & -0.910 \\ 0.000 & -0.357 & -0.934 \end{bmatrix} \tag{4.34}$$

4.7.2.2 B Matrix

The following is the result of matrix B with each row equal to $vis_i^t(\theta_i, \phi_i, \alpha, \beta)R_y(-\theta_i)$ and $\begin{bmatrix} \sin(\alpha)\cos(\phi_i + \beta) & \sin(\phi_i + \beta) & -\cos(\alpha)\cos(\phi_i + \beta) \end{bmatrix}$ using parameter from section 4.7.1

$$B = \begin{bmatrix} 0.005 & -0.617 & -0.786 \\ 0.006 & -0.358 & -0.933 \\ 0.006 & -0.362 & -0.931 \\ 0.006 & -0.518 & -0.855 \\ 0.006 & -0.415 & -0.909 \\ 0.005 & -0.621 & -0.783 \\ 0.005 & -0.537 & -0.843 \\ 0.006 & -0.376 & -0.926 \\ 0.006 & -0.418 & -0.908 \\ 0.007 & -0.361 & -0.932 \end{bmatrix} \tag{4.35}$$

4.7.2.3 Personal Eye Parameter Matrix, R

The following is the result of matrix R, using the α and β parameter.

$$R = \begin{bmatrix} \cos(\alpha) & -\sin(\alpha)\sin(\beta) & -\sin(\alpha)\cos(\beta) \\ 0 & \cos(\beta) & -\sin(\beta) \\ \sin(\alpha) & \cos(\alpha)\sin(\beta) & \cos(\alpha)\cos(\beta) \end{bmatrix} = \begin{bmatrix} 0.999 & 0.000 & -0.007 \\ 0.000 & 0.999 & -0.005 \\ 0.006 & -0.004 & -0.999 \end{bmatrix} \tag{4.36}$$

4.7.2.4 SVD of Measurement Matrix, A

The following are the result of taking the singular value decomposition of A,

$$UD = \begin{bmatrix} 0.982 & -0.184 & 0.000 \\ 0.993 & 0.113 & 0.000 \\ 0.994 & 0.108 & 0.000 \\ 0.997 & -0.064 & 0.000 \\ 0.998 & 0.050 & 0.000 \\ 0.981 & -0.190 & 0.000 \\ 0.996 & -0.088 & 0.000 \\ 0.995 & 0.093 & 0.000 \\ 0.998 & 0.047 & 0.000 \\ 0.994 & 0.109 & 0.000 \end{bmatrix} \tag{4.37}$$

$$V^t = \begin{bmatrix} 0.000 & -0.457 & -0.889 \\ 0.000 & 0.889 & -0.457 \\ -1.000 & 0.000 & 0.000 \end{bmatrix} \tag{4.38}$$

From equation (4.38), we can identify the structure of UD and V^t as the following,

$$\begin{bmatrix} \cos(\phi_i + \eta) & \sin(\phi_i + \eta) & 0 \end{bmatrix} \begin{bmatrix} 0 & -\sin(\eta) & -\cos(\eta) \\ 0 & \cos(\eta) & -\sin(\eta) \\ -1 & 0 & 0 \end{bmatrix} \tag{4.39}$$

Using analysis from section 4.6.4, evaluating equation (4.33) resulted in $\beta = 27.2$.

The ground truth subject specific parameter are $\alpha = 0.3987$ and $\beta = -0.2810$. From taking the singular value decomposition of matrix A, the information gained is the β parameter equal to 27.2. It is clear that the recovered β does not match the ground truth data. This problem will be addressed in future research.

4.8 Chapter Conclusion

From this feasibility study, we systemically developed a mathematical model for eye gaze tracking from a single camera without explicit calibration. We developed the analytic relationships between the optical axis, the visual axis and the personal eye parameters. Using this mathematical model, we showed that a measurement matrix resulting from a collection of optical axes can be constructed and factorized into the product of two matrices, one composed of the visual axes and another composed of the personal parameter only. The analytical equation of the SVD factorization of the measurement matrix is derived. We also introduced a method that maps the measurement matrix A to the subject specific rotation matrix R, based on which we can derive the personal eye parameters. Current research from simulation shows that the recovered eye parameters doesn't match the ground truth eye parameter and further research is therefore needed to address this discrepancy.

CHAPTER 5
Conclusion

5.1 Summary of Contributions

This thesis addresses the implicit calibration process of the 3D eye tracking system in two ways.

First, we extend and improve an existing stereo eye tracking approach that does not require explicit personal calibration. Alleviating problems associated with the binocular constraint, we proposed to enhance the method, with two additional constraints: the screen constraint and the eye parameter constraint. Experiments show that our method improves the existing approach and is comparable to the result of the explicit calibration process.

Second, we study the feasibility of performing calibration-free eye tracking from a monocular camera. We developed the mathematical model that establishes a concise and analytic relationship between the optical axis, the visual axis and the personal eye parameters. Using this mathematical model, we show that a measurement matrix resulting from a collection of optical axes can be constructed and furthermore the measurement matrix can be factorized into the product of two matrices- one is composed of the visual axes and another composed of the personal parameters only. Through the singular value decomposition (SVD), we introduce a method that allows us to recover the person-specific matrix.

5.2 Future Research

Based on the findings and experimental results in this research, future research can focus on improving each technique by considering different configurations, other unexplored information and further mathematical derivation.

First, the constraint-based stereo eye tracking approach will be applied to the eye tracking system with other configurations such as eye tracking system without the use of active lights. In addition, different constraints will be exploited to improve the approach. One of the possible constraints is the dynamics of the gaze trajectory.

By exploiting general prior knowledge on how the eye dynamically scans across a context, the information could be exploited for implicit calibration.

Second, we need further investigation into the second approach as to why the recovered personal parameters don't match with the groundtruth values. In addition, the stereo eye tracking system could be considered in this approach. By factorizing the appropriate measurement matrix that exploits the anatomical relationship of the two eyes, insights into the personal eye parameter could be found. Furthermore, the difference of the optical axes could be considered as the measurement matrix. The dynamics of the gaze is a feature that is not yet utilized in the gaze research community.

LITERATURE CITED

[1] D. Beymer and M. Flickner. Eye gaze tracking using an active stereo head. In *Proceeding IEEE Computer Society Conference on Computer Vision and Pattern Recognition (CVPR)*, vol. 2, 2003, pp. 451-458.

[2] R. Byrd, J. Gilbert, and J. Nocedal. A Trust Region Method Based on Interior Point Techniques for Nonlinear Programming. In *Mathematical Programming*, vol. 89, 2000, pp. 149-185.

[3] J. Chen and Q. Ji. Probabilistic gaze estimation without active personal calibration. In *Proceeding IEEE Computer Society Conference on Computer Vision and Pattern Recognition (CVPR)*, 2011, pp. 609-616.

[4] J. Chen, Y. Tong, W. Gray, and Q. Ji. A robust 3d eye gaze tracking system using noise reduction. In *Proceeding ACM Conference on Eye Tracking Research and Applications (ETRA)*, 2008, pp. 189-196.

[5] J. Favreau. "Iron Man" (2008,May) [Online], http://www.imdb.com/title/tt0371746/, Date Last Accessed, July, 15, 2011.

[6] E.D. Guestrin and M. Eizenman. Remote point-of-gaze estimation requiring a single-point calibration for applications with infants. In *Proceeding ACM Conference on Eye Tracking Research and Application (ETRA)*, 2008, pp. 267-274.

[7] E.D. Guestrin and M. Eizenman. General theory of remote gaze estimation using the pupil center and corneal reflections. In *IEEE Transaction on Biomedical Engineering*, vol. 6, 2006, pp. 1124-1133.

[8] Q. Ji and Z. Zhu. Eye and gaze tracking for interactive graphic display. In *Machine Vision and Applications*, vol.15, 2002, pp. 139-148.

[9] L.T.Inc. http://eyegaze.com, Date Last Accessed, July, 15, 2011.

[10] W. Maio, J. Chen, and Q. Ji. Constraint-based gaze estimation without active calibration. In *Proceeding IEEE Conference on Automatic Face Gesture Recognition and Workshops (FG)*, 2011, pp. 627-631.

[11] D. Model, E. Guestrin, and M. Eizenman. An automatic calibration procedure for remote eye-gaze tracking systems. In *Proceeding IEEE Conference On Engineering in Medicine and Biology Society (EMBS)*, 2009, pp. 4751-4754.

[12] C. Morimoto, A. Amir, and M. Flickner. Detecting eye position and gaze from a single camera and 2 light sources. In *International Conference on Pattern Recognition (ICPR)*, vol. 4, 2002, pp. 314-317.

[13] C. Morimoto and M. Marcio. Eye gaze tracking techniques for interactive applications. In *Computer Vision and Image Understanding*, vol. 98, 2005, pp. 4-24.

[14] S. Shih and J. Liu. A novel approach to 3-d gaze tracking using stereo cameras. In *IEEE Transactions on Systems, Man, and Cybernetics, Part B: Cybernetics*, vol. 34, 2004, pp.234-245.

[15] J. Shotton, A. Fitzgibbon, M. Cook, T. Sharp, M. Finocchio, R. Moore, A. Kipman, and A. Blake. Real-time human pose recognition in parts from a single depth image. In *Proceeding IEEE Computer Society Conference on Computer Vision and Pattern Recognition (CVPR)*, 2011, pp. 1297-1304.

[16] S. Spielberg. Minority report, June 2002. http://www.imdb.com/title/tt0181689/, Date Last Accessed, July, 15, 2011.

[17] Y. Sugano, Y. Matsushita, and Y. Sato. Calibration-free gaze sensing using saliency maps. In *Proceeding IEEE Computer Society Conference on Computer Vision and Pattern Recognition (CVPR)*, 2010, pp. 2667-2674.

[18] Y. Sugano, Y. Matsushita, Y. Sato, and H. Koike. An incremental learning method for unconstrained gaze estimation. In *European Conference On Computer Vision (ECCV)*, vol. 3, 2008 pp. 656-667.

[19] K. Tan, D. Kriegman, and N. Ahuja. Appearance-based eye gaze estimation. In *Proceeding IEEE Conference On Applications of Computer Vision (WACV)*, 2002, pp. 191-195.

[20] Graffiti Research Lab the Free Art & Technology Lab and OpenFrameworks. Eyewriter, 2009. http://www.eyewriter.org/ , Date Last Accessed, July, 15, 2011.

[21] Tobii. Tobii, 2011. http://www.tobii.com/, Date Last Accessed, July, 15, 2011.

[22] Z. Zhu, Q. Ji, and K. Bennett. Nonlinear eye gaze mapping function estimation via support vector regression. In *International Conference On Pattern Recognition (ICPR)*, vol. 1, 2006, pp. 1132-1135.

APPENDIX A
Rotation Matrices Representation of Optical Axis and Visual Axis

A.1 Optical Axis Verification

The rotation matrices representation of equation(4.3) is verified in this section.

$$\begin{aligned}\vec{op} &= \begin{bmatrix} \cos(\phi)\sin(\theta) \\ \sin(\phi) \\ -\cos(\phi)\cos(\theta) \end{bmatrix} = R_y(-\theta)R_x(\phi) \begin{bmatrix} 0 \\ 0 \\ -1 \end{bmatrix} \\ &= \begin{pmatrix} \cos(\theta) & 0 & -\sin(\theta) \\ 0 & 1 & 0 \\ \sin(\theta) & 0 & \cos(\theta) \end{pmatrix} \begin{pmatrix} 1 & 0 & 0 \\ 0 & \cos(\phi) & -\sin(\phi) \\ 0 & \sin(\phi) & \cos(\phi) \end{pmatrix} \begin{bmatrix} 0 \\ 0 \\ -1 \end{bmatrix}\end{aligned} \tag{A.1}$$

First, the z axis $\begin{bmatrix} 0 \\ 0 \\ -1 \end{bmatrix}$ is multiplied by the rotation matrix that rotates about the x-axis in equation (A.1)

$$\vec{op} = \begin{pmatrix} \cos(\theta) & 0 & -\sin(\theta) \\ 0 & 1 & 0 \\ \sin(\theta) & 0 & \cos(\theta) \end{pmatrix} \begin{bmatrix} 0 \\ \sin(\phi) \\ -\cos(\phi) \end{bmatrix} \tag{A.2}$$

Then, the axis , $\begin{bmatrix} 0 \\ \sin(\phi) \\ -\cos(\phi) \end{bmatrix}$, is multiplied by the rotation matrix that rotation about the y-axis in the inverse direction in equation A.2

$$\vec{op} = \begin{bmatrix} \cos(\phi)\sin(\theta) \\ \sin(\phi) \\ -\cos(\phi)\cos(\theta) \end{bmatrix} \tag{A.3}$$

A.2 Visual Axis Verification

Similar to section (A.1), the rotation matrices representation of equation (4.4) is verified in this section.

$$
\begin{aligned}
\vec{vis} &= \begin{bmatrix} \cos(\phi+\beta)\sin(\theta+\alpha) \\ \sin(\phi+\beta) \\ -\cos(\phi+\beta)\cos(\theta+\alpha) \end{bmatrix} = R_y(-\theta)R_y(-\alpha)R_x(\phi)R_x(\beta)\begin{bmatrix} 0 \\ 0 \\ -1 \end{bmatrix} \\
&= \begin{pmatrix} \cos(\theta) & 0 & -\sin(\theta) \\ 0 & 1 & 0 \\ \sin(\theta) & 0 & \cos(\theta) \end{pmatrix}\begin{pmatrix} \cos(\alpha) & 0 & -\sin(\alpha) \\ 0 & 1 & 0 \\ \sin(\alpha) & 0 & \cos(\alpha) \end{pmatrix}\begin{pmatrix} 1 & 0 & 0 \\ 0 & \cos(\phi) & -\sin(\phi) \\ 0 & \sin(\phi) & \cos(\phi) \end{pmatrix}\cdots \\
&\quad \begin{pmatrix} 1 & 0 & 0 \\ 0 & \cos(\beta) & -\sin(\beta) \\ 0 & \sin(\beta) & \cos(\beta) \end{pmatrix}\begin{bmatrix} 0 \\ 0 \\ -1 \end{bmatrix} \\
&= \begin{pmatrix} \cos(\theta) & 0 & -\sin(\theta) \\ 0 & 1 & 0 \\ \sin(\theta) & 0 & \cos(\theta) \end{pmatrix}\begin{pmatrix} \cos(\alpha) & 0 & -\sin(\alpha) \\ 0 & 1 & 0 \\ \sin(\alpha) & 0 & \cos(\alpha) \end{pmatrix}\begin{pmatrix} 1 & 0 & 0 \\ 0 & \cos(\phi) & -\sin(\phi) \\ 0 & \sin(\phi) & \cos(\phi) \end{pmatrix}\begin{bmatrix} 0 \\ \sin(\beta) \\ -\cos(\beta) \end{bmatrix} \\
&= \begin{pmatrix} \cos(\theta) & 0 & -\sin(\theta) \\ 0 & 1 & 0 \\ \sin(\theta) & 0 & \cos(\theta) \end{pmatrix}\begin{pmatrix} \cos(\alpha) & 0 & -\sin(\alpha) \\ 0 & 1 & 0 \\ \sin(\alpha) & 0 & \cos(\alpha) \end{pmatrix}\begin{bmatrix} 0 \\ \cos(\phi)\sin(\beta)+\sin(\phi)\cos(\beta) \\ \sin(\phi)\sin(\beta)-\cos(\phi)cos(\beta) \end{bmatrix} \\
&= \begin{pmatrix} \cos(\theta) & 0 & -\sin(\theta) \\ 0 & 1 & 0 \\ \sin(\theta) & 0 & \cos(\theta) \end{pmatrix}\begin{pmatrix} \cos(\alpha) & 0 & -\sin(\alpha) \\ 0 & 1 & 0 \\ \sin(\alpha) & 0 & \cos(\alpha) \end{pmatrix}\begin{bmatrix} 0 \\ \sin(\phi+\beta) \\ -\cos(\phi+\beta) \end{bmatrix} \\
&= \begin{pmatrix} \cos(\theta) & 0 & -\sin(\theta) \\ 0 & 1 & 0 \\ \sin(\theta) & 0 & \cos(\theta) \end{pmatrix}\begin{bmatrix} \sin(\alpha)\cos(\phi+\beta) \\ \sin(\phi+\beta) \\ -\cos(\alpha)\cos(\phi+\beta) \end{bmatrix} \\
&= \begin{bmatrix} \cos(\theta)\sin(\alpha)\cos(\phi+\beta)+\sin(\theta)\cos(\alpha)\cos(\phi+\beta) \\ \sin(\phi+\beta) \\ \sin(\theta)\sin(\alpha)\cos(\phi+\beta)-\cos(\theta)\cos(\alpha)\cos(\phi+\beta) \end{bmatrix} \\
&= \begin{bmatrix} \sin(\theta+\alpha)\cos(\phi+\beta) \\ \sin(\phi+\beta) \\ -\cos(\theta+\alpha)\cos(\phi+\beta) \end{bmatrix}
\end{aligned}
\tag{A.4}
$$

APPENDIX B
Rotation Matrix Property

B.1 Same-Axis Rotation Matrix Commutative Property

This sections proves the commutative property of rotation matrices with the same rotation axis.

$$R_x(\theta_1 + \theta_2) = R_x(\theta_1)R_x(\theta_2) = R_x(\theta_2)R_x(\theta_1) \tag{B.1}$$

The equation above is commutative, since $R_x(\theta_1 + \theta_2) = R_x(\theta_2 + \theta_1)$. The following equations proves that equation (B.1) is true.

$$\begin{aligned}
R_x(\theta_1)R_x(\theta_2) &= \begin{bmatrix} 1 & 0 & 0 \\ 0 & \cos(\theta_1) & \sin(\theta_1) \\ 0 & -\sin(\theta_1) & \cos(\theta_1) \end{bmatrix} \begin{bmatrix} 1 & 0 & 0 \\ 0 & \cos(\theta_2) & \sin(\theta_2) \\ 0 & -\sin(\theta_2) & \cos(\theta_2) \end{bmatrix} \\
&= \begin{bmatrix} 1 & 0 & 0 \\ 0 & \cos(\theta_1)\cos(\theta_2) - \sin(\theta_1)\sin(\theta_2) & \cos(\theta_1)\sin(\theta_2) + \sin(\theta_1)\cos(\theta_2) \\ 0 & -\sin(\theta_1)\cos(\theta_2) - \cos(\theta_1)\sin(\theta_2) & -\sin(\theta_1)\sin(\theta_2) + \cos(\theta_1)\cos(\theta_2) \end{bmatrix} \\
&= \begin{bmatrix} 1 & 0 & 0 \\ 0 & \cos(\theta_1 + \theta_2) & \sin(\theta_1 + \theta_2) \\ 0 & -\sin(\theta_1 + \theta_2) & \cos(\theta_1 + \theta_2) \end{bmatrix} \\
&= R_x(\theta_1 + \theta_2) \\
&= \begin{bmatrix} 1 & 0 & 0 \\ 0 & \cos(\theta_2) & \sin(\theta_2) \\ 0 & -\sin(\theta_2) & \cos(\theta_2) \end{bmatrix} \begin{bmatrix} 1 & 0 & 0 \\ 0 & \cos(\theta_1) & \sin(\theta_1) \\ 0 & -\sin(\theta_1) & \cos(\theta_1) \end{bmatrix} \\
&= R_x(\theta_2)R_x(\theta_1)
\end{aligned} \tag{B.2}$$

From equation (B.2), it is valid that the order rotation angles rotating about the same axis is interchangeable.

B.2 Rotation Matrix Inverse Property

The transpose of a rotation matrix is the equivalent of rotating in the opposite direction. The following equation demonstrates the concept.

$$R^t(\theta) = R(-\theta) \tag{B.3}$$

To prove equation (B.3), the rotation matrix, rotating about the x-axis is used. Initially, we have the x-axis rotation matrix.

$$R_x(\theta) = \begin{bmatrix} 1 & 0 & 0 \\ 0 & \cos(\theta) & \sin(\theta) \\ 0 & -\sin(\theta) & \cos(\theta) \end{bmatrix} \tag{B.4}$$

Taking the transpose of equation (B.4), we have the following equation,

$$R_x^t(\theta) = \begin{bmatrix} 1 & 0 & 0 \\ 0 & \cos(\theta) & -\sin(\theta) \\ 0 & \sin(\theta) & \cos(\theta) \end{bmatrix} \tag{B.5}$$

Equivalently, if a negative rotation angle is applied, the resulting matrix is the same as equation (B.5) using the trigonometry identities.

$$\begin{aligned} R_x(-\theta) &= \begin{bmatrix} 1 & 0 & 0 \\ 0 & \cos(-\theta) & \sin(-\theta) \\ 0 & -\sin(-\theta) & \cos(-\theta) \end{bmatrix} \\ &= \begin{bmatrix} 1 & 0 & 0 \\ 0 & \cos(\theta) & -\sin(\theta) \\ 0 & \sin(\theta) & \cos(\theta) \end{bmatrix} \end{aligned} \tag{B.6}$$

APPENDIX C
Rotation Matrix Evaluation for A and B

C.1 A Matrix Evaluation

In this section, the parametrization of equation (4.11), each row of A, is verified.

$$A_i = \vec{op}^t R_y(-\theta_i) = \begin{bmatrix} 0 & 0 & -1 \end{bmatrix} R_x(-\phi_i) R_y(\theta_i) R_y(-\theta_i) = \begin{bmatrix} 0 & \sin(\phi_i) & -\cos(\phi_i) \end{bmatrix} \tag{C.1}$$

Expanding the rotation matrices of equation (C.1), we have the following equation,

$$\begin{bmatrix} 0 & 0 & -1 \end{bmatrix} \begin{bmatrix} 1 & 0 & 0 \\ 0 & \cos(\phi_i) & \sin(\phi_i) \\ 0 & -\sin(\phi_i) & \cos(\phi_i) \end{bmatrix} \begin{bmatrix} \cos(\theta_i) & 0 & \sin(\theta_i) \\ 0 & 1 & 0 \\ -\sin(\theta_i) & 0 & \cos(\theta_i) \end{bmatrix} \begin{bmatrix} \cos(\theta_i) & 0 & \sin(-\theta_i) \\ 0 & 1 & 0 \\ -\sin(-\theta_i) & 0 & \cos(-\theta_i) \end{bmatrix} \tag{C.2}$$

From equation (C.2), the rotation matrices about the y-axis are canceled because the two angles are equal and opposite. Evaluating the following equation, we have the resulting equation (C.1)

$$\vec{op}^t R_y(-\theta_i) = \begin{bmatrix} 0 & 0 & -1 \end{bmatrix} \begin{bmatrix} 1 & 0 & 0 \\ 0 & \cos(\phi_i) & \sin(\phi_i) \\ 0 & -\sin(\phi_i) & \cos(\phi_i) \end{bmatrix} = \begin{bmatrix} 0 & \sin(\phi_i) & -\cos(\phi_i) \end{bmatrix} \tag{C.3}$$

C.2 B Matrix Evaluation

Similar to section C.1, the B matrix is evaluated in this section. From equation (4.12), we have the following equation,

$$\begin{aligned} B_i = \vec{vis}^{\,t} R_y(-\theta_i) &= \begin{bmatrix} 0 & 0 & -1 \end{bmatrix} R_x(-\phi_i) R_x(-\beta) R_y(\alpha) R_y(\theta_i) R_y(-\theta_i) \\ &= \begin{bmatrix} \sin(\alpha)\cos(\phi_i+\beta) & \sin(\phi_i+\beta) & -\cos(\alpha)\cos(\phi_i+\beta) \end{bmatrix} \end{aligned} \tag{C.4}$$

The following equation evaluates equation (4.12) explicitly.

$$
\begin{aligned}
\vec{vis}^{\,t} R_y(-\theta_i) &= \begin{bmatrix} 0 & 0 & -1 \end{bmatrix} R_x(-\phi) R_x(-\beta) R_y(\alpha) R_y(\theta) R_y(-\theta) \\
&= \begin{bmatrix} 0 & 0 & -1 \end{bmatrix} \begin{bmatrix} 1 & 0 & 0 \\ 0 & \cos(\phi_i) & \sin(\phi_i) \\ 0 & -\sin(\phi_i) & \cos(\phi_i) \end{bmatrix} \begin{bmatrix} 1 & 0 & 0 \\ 0 & \cos(\beta) & \sin(\beta) \\ 0 & -\sin(\beta) & \cos(\beta) \end{bmatrix} \begin{bmatrix} \cos(\alpha) & 0 & \sin(\alpha) \\ 0 & 1 & 0 \\ -\sin(\alpha) & 0 & \cos(\alpha) \end{bmatrix} \\
&= \begin{bmatrix} 0 & \sin(\phi_i) & -\cos(\phi_i) \end{bmatrix} \begin{bmatrix} 1 & 0 & 0 \\ 0 & \cos(\beta) & \sin(\beta) \\ 0 & -\sin(\beta) & \cos(\beta) \end{bmatrix} \begin{bmatrix} \cos(\alpha) & 0 & \sin(\alpha) \\ 0 & 1 & 0 \\ -\sin(\alpha) & 0 & \cos(\alpha) \end{bmatrix} \\
&= \begin{bmatrix} 0 & \sin(\phi_i + \beta) & -\cos(\phi_i + \beta) \end{bmatrix} \begin{bmatrix} \cos(\alpha) & 0 & \sin(\alpha) \\ 0 & 1 & 0 \\ -\sin(\alpha) & 0 & \cos(\alpha) \end{bmatrix} \\
&= \begin{bmatrix} \sin(\alpha)\cos(\phi_i + \beta) & \sin(\phi_i + \beta) & -\cos(\alpha)\cos(\phi_i + \beta) \end{bmatrix}
\end{aligned}
\tag{C.5}
$$

APPENDIX D
Rank Analysis of A, B, and R

D.1 A Matrix

Each row of matrix A has the following structure $\begin{bmatrix} 0 & \sin(\phi_i) & -\cos(\phi_i) \end{bmatrix}$ From each row of A, it is clear that all of the elements in the first column of A are zero. Since the second and third column of A are parameterized by non-linear functions with ϕ angle, then the number of linearly independent column vector for A is two, thus rank of A must be 2.

D.2 B Matrix

Since the rank of B cannot be clearly observed from the rows of B, the determinant of 3 sample rows of B matrix is tested to determine whether all of the rows

are linearly independent.

$$
\begin{aligned}
\det(B_{1,2,3}) &= \det \begin{bmatrix} \sin(\alpha)\cos(\phi_1+\beta) & \sin(\phi_1+\beta) & -\cos(\alpha)\cos(\phi_1+\beta) \\ \sin(\alpha)\cos(\phi_2+\beta) & \sin(\phi_2+\beta) & -\cos(\alpha)\cos(\phi_2+\beta) \\ \sin(\alpha)\cos(\phi_3+\beta) & \sin(\phi_3+\beta) & -\cos(\alpha)\cos(\phi_3+\beta) \end{bmatrix} \\
&= \sin(\alpha)\cos(\phi_1+\beta) \begin{bmatrix} \sin(\phi_2+\beta) & -\cos(\alpha)\cos(\phi_2+\beta) \\ \sin(\phi_3+\beta) & -\cos(\alpha)\cos(\phi_3+\beta) \end{bmatrix} \\
&- \sin(\phi_1+\beta) \begin{bmatrix} \sin(\alpha)\cos(\phi_2+\beta) & -\cos(\alpha)\cos(\phi_2+\beta) \\ \sin(\alpha)\cos(\phi_3+\beta) & -\cos(\alpha)\cos(\phi_3+\beta) \end{bmatrix} \\
&- \cos(\alpha)\cos(\phi_1+\beta) \begin{bmatrix} \sin(\alpha)\cos(\phi_2+\beta) & \sin(\phi_2+\beta) \\ \sin(\alpha)\cos(\phi_3+\beta) & \sin(\phi_3+\beta) \end{bmatrix} \\
&= \sin(\alpha)\cos(\phi_1+\beta)\cos(\alpha)(-\sin(\phi_2+\beta)\cos(\phi_3+\beta)+\cos(\phi_2+\beta)\sin(\phi_3+\beta)) \\
&- \sin(\phi_1+\beta)\sin(\alpha)\cos(\alpha)(-\cos(\phi_2+\beta)\cos(\phi_3+\beta)+\cos(\phi_2+\beta)\cos(\phi_3+\beta)) \\
&- \cos(\alpha)\cos(\phi_1+\beta)\sin(\alpha)(\cos(\phi_2+\beta)\sin(\phi_3+\beta)-\sin(\phi_2+\beta)\cos(\phi_3+\beta)) \\
&= \sin(\alpha)\cos(\phi_1+\beta)\cos(\alpha)(\sin(\phi_3+\beta-\phi_2-\beta)) \\
&- \cos(\alpha)\cos(\phi_1+\beta)\sin(\alpha)(\sin(\phi_3+\beta-\phi_2-\beta)) \\
&= \sin(\alpha)\cos(\alpha)\cos(\phi_1+\beta)(\sin(\phi_3-\phi_2)-\sin(\phi_3-\phi_2)) = 0
\end{aligned}
\tag{D.1}
$$

Since the determinant of 3 rows of matrix B is zero, this means that the columns are linearly dependent. The linear dependency can be observed from the equation, since the α parameter of each row is constant, the difference between the first column and third column of B is the scale factor that is a function of α.

D.3 R Matrix

Similar to determining the rank of B, the determinant of R is taken to determine if each of the columns are linearly independent.

$$
\begin{aligned}
det(R) &= det \begin{bmatrix} \cos(\alpha) & -\sin(\alpha)\sin(\beta) & -\sin(\alpha)\cos(\beta) \\ 0 & \cos(\beta) & -\sin(\beta) \\ \sin(\alpha) & \cos(\alpha)\sin(\beta) & \cos(\alpha)\cos(\beta) \end{bmatrix} \\
&= \cos(\alpha)[\cos(\beta)\cos(\alpha)\cos(\beta) + \sin(\beta)\cos(\alpha)\sin(\beta)] \\
&+ \sin(\alpha)\sin(\beta)\sin(\beta)\sin(\alpha) + \sin(\alpha)\cos(\beta)\cos(\beta)\sin(\alpha) \\
&= \cos^2(\alpha)\cos^2(\beta) + \cos^2(\alpha)\sin^2(\beta) + \sin^2(\alpha)\sin^2(\beta) + \sin^2(\alpha)\cos^2(\beta) \\
&= \cos^2(\alpha)(\cos^2(\beta) + \sin^2(\beta)) + \sin^2(\alpha)(\cos^2(\beta) + \sin^2(\beta)) = 1
\end{aligned}
\tag{D.2}
$$

The determinant of R is 1, therefore each of the rows and columns are linearly independent, thus the rank of R is 3.

APPENDIX E
Singular Value Decomposition Parameterization

From the result of the singular value decomposition of matrix A (UD and V^t), there is a distinct pattern in the data. The structure of the result can be characterized by a parameter η that is added to the ϕ parameter in each row of A. The general structure of UD and V^t is the following.

$$UD = \begin{bmatrix} \pm\cos(\phi \pm \eta) & \pm\sin(\phi \pm \eta) & 0 \end{bmatrix} \tag{E.1}$$

$$V^t = \begin{bmatrix} 0 & \pm\sin(\eta) & \pm\cos(\eta) \\ 0 & \pm\cos(\eta) & \pm\sin(\eta) \\ 1 & 0 & 0 \end{bmatrix} \tag{E.2}$$

Regardless of the signs of the structure, the multiplication of each of the rows must equal $\begin{bmatrix} 0 & \sin(\phi_i) & -\cos(\phi_i) \end{bmatrix}$. Limiting the angle variation of η from 0 to 90, the sign of the structure is dependent on the signs of each of the element on Vt. For example, if the following Vt is observed, $\begin{bmatrix} 0 & v_{12} & -v_{13} \\ 0 & -v_{22} & -v_{23} \\ 1 & 0 & 0 \end{bmatrix}$, the following is the corresponding structure.

$$\begin{bmatrix} \cos(\phi_i - \eta) & -\sin(\phi_i - \eta) & 0 \end{bmatrix} \begin{bmatrix} 0 & \sin(\eta) & -\cos(\eta) \\ 0 & -\cos(\eta) & -\sin(\eta) \\ 1 & 0 & 0 \end{bmatrix} = \begin{bmatrix} 0 & \sin(\phi_i) & -\cos(\phi_i) \end{bmatrix} \tag{E.3}$$

Following equation (E.3), the following are the other possible structures.

$$\begin{bmatrix} -\cos(\phi_i - \eta) & -\sin(\phi_i - \eta) & 0 \end{bmatrix} \begin{bmatrix} 0 & -\sin(\eta) & \cos(\eta) \\ 0 & -\cos(\eta) & -\sin(\eta) \\ 1 & 0 & 0 \end{bmatrix} = \begin{bmatrix} 0 & \sin(\phi_i) & -\cos(\phi_i) \end{bmatrix} \tag{E.4}$$

$$\begin{bmatrix}\cos(\phi_i+\eta) & \sin(\phi_i+\eta) & 0\end{bmatrix}\begin{bmatrix}0 & -\sin(\eta) & -\cos(\eta)\\ 0 & \cos(\eta) & -\sin(\eta)\\ 1 & 0 & 0\end{bmatrix}=\begin{bmatrix}0 & \sin(\phi_i) & -\cos(\phi_i)\end{bmatrix} \tag{E.5}$$

$$\begin{bmatrix}\cos(\phi_i+\eta) & -\sin(\phi_i+\eta) & 0\end{bmatrix}\begin{bmatrix}0 & -\sin(\eta) & -\cos(\eta)\\ 0 & -\cos(\eta) & \sin(\eta)\\ 1 & 0 & 0\end{bmatrix}=\begin{bmatrix}0 & \sin(\phi_i) & -\cos(\phi_i)\end{bmatrix} \tag{E.6}$$

$$\begin{bmatrix}-\cos(\phi_i-\eta) & \sin(\phi_i-\eta) & 0\end{bmatrix}\begin{bmatrix}0 & -\sin(\eta) & \cos(\eta)\\ 0 & \cos(\eta) & \sin(\eta)\\ 1 & 0 & 0\end{bmatrix}=\begin{bmatrix}0 & \sin(\phi_i) & -\cos(\phi_i)\end{bmatrix} \tag{E.7}$$

$$\begin{bmatrix}\cos(\phi_i-\eta) & \sin(\phi_i-\eta) & 0\end{bmatrix}\begin{bmatrix}0 & \sin(\eta) & -\cos(\eta)\\ 0 & \cos(\eta) & \sin(\eta)\\ 1 & 0 & 0\end{bmatrix}=\begin{bmatrix}0 & \sin(\phi_i) & -\cos(\phi_i)\end{bmatrix} \tag{E.8}$$

$$\begin{bmatrix}-\cos(\phi_i+\eta) & -\sin(\phi_i+\eta) & 0\end{bmatrix}\begin{bmatrix}0 & \sin(\eta) & \cos(\eta)\\ 0 & -\cos(\eta) & \sin(\eta)\\ 1 & 0 & 0\end{bmatrix}=\begin{bmatrix}0 & \sin(\phi_i) & -\cos(\phi_i)\end{bmatrix} \tag{E.9}$$

$$\begin{bmatrix} -\cos(\phi_i + \eta) & \sin(\phi_i + \eta) & 0 \end{bmatrix} \begin{bmatrix} 0 & \sin(\eta) & \cos(\eta) \\ 0 & \cos(\eta) & -\sin(\eta) \\ 1 & 0 & 0 \end{bmatrix} = \begin{bmatrix} 0 & \sin(\phi_i) & -\cos(\phi_i) \end{bmatrix} \tag{E.10}$$

The η angle is a piece of information that is created from taking the singular value decomposition of matrix A. The theory is that this angle has some connection to the subject specific parameter.

APPENDIX F
η Parameter Verification

In this chapter, the solution of V^t from the SVD of the measurement matrix A is verified analytically by solving for the η parameter. From numerical simulation in section 4.6.3, one of the possible configuration of V^t has the following structure,

$$V^t = \begin{bmatrix} 0 & \sin(\eta) & -\cos(\eta) \\ 0 & \cos(\eta) & \sin(\eta) \\ 1 & 0 & 0 \end{bmatrix} \tag{F.1}$$

From the definition of the eigenvectors, we have the following equation,

$$((A^tA)v - \lambda_{eig}v) = 0 \tag{F.2}$$

where v is one of the eigenvectors. When the eigenvalue of A^tA is 0, the corresponding eigenvector is $\begin{bmatrix} 1 \\ 0 \\ 0 \end{bmatrix}$, which was observed from the numerical analysis. To simplify the analysis, the summation of $\cos(2\phi_i)$ and $\sin(2\phi_i)$ are replaced with symbols d and e.

$$d = \sum_{i=1}^{i=N} \cos(2\phi_i) \tag{F.3}$$

$$e = \sum_{i=1}^{i=N} \sin(2\phi_i) \tag{F.4}$$

The derivation is given in the following equation,

$$\begin{bmatrix} 0 & 0 & 0 \\ 0 & \frac{1}{2}(N-d) & -\frac{1}{2}e \\ 0 & -\frac{1}{2}e & \frac{1}{2}(N+d) \end{bmatrix} \begin{bmatrix} 1 \\ 0 \\ 0 \end{bmatrix} - \begin{bmatrix} \lambda_{eigen} & 0 & 0 \\ 0 & \lambda_{eigen} & 0 \\ 0 & 0 & \lambda_{eigen} \end{bmatrix} \begin{bmatrix} 1 \\ 0 \\ 0 \end{bmatrix} = 0$$

$$\begin{bmatrix} -\lambda_{eigen} & 0 & 0 \\ 0 & \frac{1}{2}(N-d) - \lambda_{eigen} & -\frac{1}{2}e \\ 0 & -\frac{1}{2}e & \frac{1}{2}(N+d) - \lambda_{eigen} \end{bmatrix} \begin{bmatrix} 1 \\ 0 \\ 0 \end{bmatrix} = 0 \tag{F.5}$$

$$\begin{bmatrix} 0 & 0 & 0 \\ 0 & \frac{1}{2}(N-d) - 0 & -\frac{1}{2}e \\ 0 & -\frac{1}{2}e & \frac{1}{2}(N+d) - 0 \end{bmatrix} \begin{bmatrix} 1 \\ 0 \\ 0 \end{bmatrix} = 0$$

Using the second row of equation F.1 for the eigenvector v, we have the following equation,

$$\begin{bmatrix} -\lambda_{eigen} & 0 & 0 \\ 0 & \frac{1}{2}(N-d) - \lambda_{eigen} & -\frac{1}{2}e \\ 0 & -\frac{1}{2}e & \frac{1}{2}(N+d) - \lambda_{eigen} \end{bmatrix} \begin{bmatrix} 0 \\ \cos(\eta) \\ \sin(\eta) \end{bmatrix} = 0 \tag{F.6}$$

The corresponding eigenvalue for the eigenvector $\begin{bmatrix} 0 \\ \cos(\eta) \\ \sin(\eta) \end{bmatrix}$ is presented in the following equation.

$$\lambda_{eig} = \frac{1}{2}N + \frac{1}{2}\sqrt{(d)^2 + (e)^2} \tag{F.7}$$

Combining the eigenvalues of equation (F.7) with equation (F.6), we can solve for η,

$$\begin{bmatrix} -\frac{1}{2}N + \frac{1}{2}\sqrt{(d)^2 + (e)^2} & 0 & 0 \\ 0 & -\frac{1}{2}d - \frac{1}{2}\sqrt{(d)^2 + (e)^2} & -\frac{1}{2}e \\ 0 & -\frac{1}{2}e & \frac{1}{2}d - \frac{1}{2}\sqrt{(d)^2 + (e)^2} \end{bmatrix} \begin{bmatrix} 0 \\ \cos(\eta) \\ \sin(\eta) \end{bmatrix} = 0 \tag{F.8}$$

$$(-\frac{1}{2}d - \frac{1}{2}\sqrt{(d)^2 + (e)^2})\cos(\eta) - \frac{1}{2}e\sin(\eta) = 0 \tag{F.9}$$

$$-\frac{1}{2}e\cos(\eta) + (\frac{1}{2}d - \frac{1}{2}\sqrt{(d)^2 + (e)^2})\sin(\eta) = 0 \tag{F.10}$$

$$\tan\eta = \frac{\sin(\eta)}{\cos(\eta)} = \frac{-d - \sqrt{(d)^2 + (e)^2}}{e} \tag{F.11}$$

$$\tan\eta = \frac{\sin(\eta)}{\cos(\eta)} = \frac{e}{d - \sqrt{(d)^2 + (e)^2}} \tag{F.12}$$

$$\eta = \tan^{-1}(\frac{-d - \sqrt{(d)^2 + (e)^2}}{e}), \tan^{-1}(\frac{e}{d - \sqrt{(d)^2 + (e)^2}}) \tag{F.13}$$

To confirm the equation derivation of η, we verify and see if both of the solution of equation (F.13) yields the same result by equating the two solutions.

$$\tan^{-1}(\frac{-d - \sqrt{(d)^2 + (e)^2}}{e}) = \tan^{-1}(\frac{e}{d - \sqrt{(d)^2 + (e)^2}}) \tag{F.14}$$

$$\frac{-d - \sqrt{(d)^2 + (e)^2}}{e} = \frac{e}{d - \sqrt{(d)^2 + (e)^2}} \tag{F.15}$$

By cross-multiplying equation (F.15), we can see that both solutions yields the same result.

$$-d^2 + d^2 + e^2 = e^2 \tag{F.16}$$

Thus, equation (F.13) parameterizes the solution for η under the assumption that parametrization from the numerical analysis of the result is correct. Further research is needed for further verification.